Determination of the Hubble constant, the intrinsic scatter of luminosities of Type Ia SNe, and evidence for non-standard dust in other galaxies

Xiaofeng Wang[1,2,3], Lifan Wang[4], Reynald Pain[3],
Xu Zhou[2], Zongwei Li[5]

ABSTRACT

A sample of 109 type Ia supernovae (SNe Ia) with recession velocity $\lesssim$ 30,000 km s^{-1}, is compiled from published SNe Ia light curves to explore the expansion rate of the local Universe. Based on the color parameter ΔC_{12} and the decline rate Δm_{15}, we found that the average absorption to reddening ratio for SN Ia host galaxies to be R_{UBVI} = 4.37±0.25, 3.33±0.11, 2.30±0.11, 1.18±0.11, which are systematically lower than the standard values in the Milky Way. We investigated the correlations of the intrinsic luminosity with light curve decline rate, color index, and supernova environmental parameters. In particular, we found SNe Ia in E/S0 galaxies to be brighter close to the central region than those in the outer region, which may suggest a possible metallicity effect on SN luminosity. The dependence of SN luminosity on galactic environment disappears after corrections for the extinction and ΔC_{12}. The Hubble diagrams constructed using 73 Hubble flow SNe Ia yield a 1-σ scatter of $\lesssim$0.12 mag in BVI bands and $\sim$0.16 mag in U band. The luminosity difference between normal SNe Ia and peculiar objects (including SN 1991bg-like and 1991T-like events) has now been reduced to within 0.15 mag via ΔC_{12} correction. We use the same precepts to correct the nearby SNe Ia with Cepheid distances and found that the fully corrected absolute magnitudes of SNe Ia are: $M_B = -19.33\pm0.06$, $M_V = -19.27\pm0.05$. We deduced a value for the Hubble constant of $H_0 = 72 \pm 6$ (total) km s^{-1} Mpc^{-1}.

[1]Physics Department and Tsinghua Center for Astrophysics (THCA), Tsinghua University, Beijing, 100084, P R China; wang_xf@mail.tsinghua.edu.cn

[2]National Astronomical Observatories of China, Chinese Academy of Sciences, Beijing 100012, P R China; wxf@vega.bac.pku.edu.cn

[3]LPNHE, CNRS-IN2P3, University of Paris VI&VII, Paris, France

[4]E.O. Lawrence Berkeley National Laboratory, 1 Cyclotron Rd., Berkeley, CA94720, USA

[5]Department of Astronomy, Beijing Normal University, 100875, Beijing, China

Subject headings: Cepheids – cosmological parameters – cosmology: observations – distance scale – dust, extinction – supernovae: general

1. Introduction

Type Ia supernovae (SNe Ia) are probably the most precise distance indicators known for measuring the extragalactic distances. Their Hubble diagram, i.e., magnitude-redshift (m-z) relation, can be used to trace the expansion history of the universe. The linear portion of the Hubble diagram with absolute magnitude calibration determines the Hubble constant (see a review in Branch 1998); curvature in the diagram probes evolution of the expansion rate, i.e., acceleration or deceleration, and consequently different combinations of the cosmological parameters such as Ω_m and Ω_Λ (Riess et al. 1998; Perlmutter et al. 1999).

Various empirical methods have been developed to calibrate the peak luminosities of SNe Ia. These include the template fitting or Δm_{15} method (Phillips 1993, Hamuy et al. 1996, Phillips et al. 1999), the multi-color light curve method shape (MLCS) method (Riess et al. 1996a; Jha 2002), and the stretch factor method (Perlmutter et al. 1997; Goldhaber et al. 2001), the "Bayesian Template Method" (BATM; Tonry et al. 2003), and the recently proposed Spectral Adaptive Light Curve (SALT) method (Guy et al. 2005). These methods are fundamentally identical by utilizing the relationship between SN Ia light curve shape and peak luminosity. The Color-Magnitude Intercept method (CMAGIC) of Wang L et al. (2003, 2005) shows some variance, which replaces the magnitude at maximum with the more uniform magnitude at a given value of the color index. The above methods can yield distances to SN Ia host galaxies with a relative precision approaching 8-11% which demonstrates the power of SNe Ia as cosmological lighthouses for extragalactic distance scales. Wang et al. (2005) recently proposed a method which is similar to the Δm_{15} method of Phillips et al. (1999), but instead of using the $B-V$ color at maximum, we proposed to using the $B-V$ color at 12 days past optical maximum as a more efficient calibration parameter.

By common practice so far, the spectroscopically peculiar SNe Ia are usually excluded or given a lower weight in cosmological studies. According to Li et al. (2001a), however, the total rate of peculiar SNe Ia in a volume-limited search could be as high as 36%. The rate of SN 1991T/1999aa-like objects is ∼20% and the rate of SN 1991bg-like objects is ∼16%. Some of the peculiar SNe Ia apparently deviate from the relation between light curve shape and luminosity. The ΔC_{12} method provides a better way to homogenize the normal SNe Ia and the spectroscopically peculiar ones in a more unified and consistent manner.

The color parameter $\Delta C_{12} = (B-V)_{12}$ gives tighter empirical relations with SN Ia peak luminosities (Wang et al. 2005; W05). Here we apply this method to study the local Hubble diagram by including different peculiar types of SNe Ia. Based on the Hubble flow SNe Ia and nearby ones with Cepheid distances, we deduce the value of the Hubble constant. In §2 we describe the data selection for this study. In §3, we derive the host galaxy reddening of SN Ia and estimate the ratios of extinction to reddening for dust in SN host galaxies. In §4 we, examine the luminosity dependence of SNe Ia on secondary parameters. In §5, we present the Hubble diagram of SNe Ia and give the best estimates of H_0. Conclusions and discussion are given in §6.

2. The Data

The major sources of SN Ia light curves are: (a) the BVI light curves of 29 SNe Ia from the earlier Calan/Tololo SN survey (CTIO sample; see Hamuy et al. 1996a,b,c), (b) the $BVRI$ light curves of 22 SNe Ia collected by the CfA (CfA I sample; see Riess et al. 1999), (c) the $UBVRI$ light curves of another 44 SNe Ia from the CfA SN monitoring campaign (CfA II sample; see Jha et al. 2006a), and (d) the Las Campanas/CTIO observing campaign which covers broad band $UBVRIJHK$ photometry (Krisciunas et al. 2001, 2003, 2004a,b).

Reindl et al. (2005; hereafter R05) compiled a sample of 124 nearby SNe Ia ($z \lesssim 0.1$). Our sample is different in that we include only SNe with CCD measurements, and those observed 8 days before maximum and with more than 5 photometric points. The sample includes 109 SNe Ia, 88 of which are spectroscopically normal (Branch et al. 1993), 13 are 91T/99aa-like (Phillips et al. 1992; Filippenko et al. 1992a; Li et al. 2001a), 6 are 91bg-like (Filippenko et al. 1992b; Leibundgut et al. 1993). For light curve fitting, we follow the template fitting procedure of Hamuy et al. (1996b) but with six additional template SNe for better Δm_{15} sampling. Besides the SN templates (viz., 1991T, 1992bc, 1992al, 1992A, 1992bo, 1991bg) initially used by Hamuy et al. (1996b), six additional SNe are included as templates: SNe 1999aa ($\Delta m_{15} = 0.82$), 1999ee($\Delta m_{15} = 0.95$), 1998aq-1998bu ($\Delta m_{15} = 1.05$), 1996X-2002er($\Delta m_{15} = 1.32$), 2000dk ($\Delta m_{15} = 1.62$), and 1999by ($\Delta m_{15} = 1.90$). These light curve templates were also used to derive the peak magnitudes in the U band. Table 1 shows the fitted parameters for this sample. They are tabulated in the following manner:

Column (1): The name of the each SN.
Column (2): The name of the corresponding host galaxy.
Column (3): The redshift in the reference frame of the cosmic microwave background (CMB), using the procedure given at NASA Extragalactic Database (NED; http://nedwww.ipac.caltech.edu/),

or for a self-consistent Virgo-centric infall vector of 220 km s^{-1} taken from R05.
Column (4)-(7): The fitted peak magnitudes in $UBVI$ bands, corrected for the Galactic reddening from Schlegel et al. (1998) and the K corrections from Nugent et al. (2002). The magnitude errors in unit of 0.01 mag were a quadrature sum of the uncertainties in the observed magnitudes, foreground reddening (0.08 mag in U, 0.06 mag in B, 0.045 mag in V, and 0.03 mag in I), as well as in the K term (assumed to be 0.02 mag).
Column (8): The decline rate Δm_{15}, corrected for the small reddening effect (Phillips et al. 1999).
Column (9): The $B-V$ color 12 days after B maximum. It was measured directly from the photometry or from the best-fit light curve template when the observed color curves were too sparse to be measured accurately. The ΔC_{12} value presented here was already corrected for the Galactic reddening.
Column (10): The Galactic reddening following Schlegel et al. (1998).
Column (11): The reddening E$(B-V)$ in the host galaxy as derived from the tail of the $B-V$ color curves.
Column (12): The reddening E$(B-V)$ in the host galaxy as determined from the post maximum color ΔC_{12} (see next section and W05).
Column (13): The adopted reddening E$(B-V)_{host}$ in the host galaxy which is the weighted average of Columns (11) and (12).
Column (14): The key reference sources of SN Ia photometry.

In Table 2, additional information is assembled for the corresponding host galaxies of the SNe Ia listed in Table 1. Columns (1)-(3) are self-explanatory. Column (4)-(5) list the morphological and coded Hubble types of the host galaxies. Column (6) gives the deprojected galactocentric distances of the SNe in their respective host galaxies in units of the galaxy radius r_{25} (taken from the work of Xu & Wang 2006 in preparation) . Column (7)-(10) give the luminosity distances to the SNe Ia (see discussion in § 5.3).

3. The Extinction Correction

The Galactic extinction are corrected by using the dust maps from Schlegel et al. (1998). We need to know the intrinsic colors of SNe to estimate the reddening by the dust in the host galaxies. This unavoidably requires assumptions on the intrinsic properties of SNe.

3.1. The colors and reddening of SNe Ia

It was shown by Lira (1995) that the intrinsic $B-V$ color evolution of SNe Ia 30−90 days past V maximum can be well approximated by a simple linear relation: $(B-V)_0 = 0.725-0.0118\times(t_V-60)$, where t_V is the time (in days) from the V maximum. By empirically assuming that the intrinsic colors of SNe at late time are all identical and follow the above relation, one can deduce the reddening from the offset of the observed "tail" color of SN Ia from the above relation. The host galaxy reddening $\mathrm{E}(B-V)_{tail}$ estimated this way are reported in column (11) of Table 1.

The "tail" color is difficult to measure accurately. In most cases, we have to use the colors at maximum or shortly after maximum, provided that their intrinsic behavior is understood. It is difficult to define a reddening-free sample of SNe. Therefore we have applied a color cut of $\mathrm{E}(B-V)_{tail} \lesssim 0.06$ mag to construct a sub-sample of 36 SNe which are likely to suffer little aborption. Figure 1 shows Δm_{15} dependence of the peak colors $U_{max}-B_{max}$, $B_{max}-V_{max}$, $V_{max}-I_{max}$, and the post maximum color ΔC_{12}. Half of these SNe are located in the dust-poor earlier-type E/S0 galaxies. 80% of the remaining half are located in the outskirts of their spiral hosts.

As shown in Figure 1, all colors show similar "kinks" near $\Delta m_{15} \sim 1.65$. A simple linear relation failed to describe the color-Δm_{15} relation for these SNe Ia. A cubic spline is employed to fit the data points in Fig.1. This results in a dispersion of 0.07-0.08 mag for BVI colors at maximum. The peak $U-B$ color shows a wider range (from about −0.6 to 0.6) for SNe with different Δm_{15}. The scatter in the $U-B$ color is also larger, e.g. ∼0.14 mag (see Jha et al. 2006a for a similar argument by using the stretch factor).

Compared to the $UBVI$ colors at maximum light, the post-maximum color parameter ΔC_{12} shows a much tighter dependence on Δm_{15}, which is given as,

$$\Delta C_{12} = 0.33_{\pm 0.01}+0.32_{\pm 0.04}(\Delta m_{15}-1.1)-0.56_{\pm 0.21}(\Delta m_{15}-1.1)^2+2.16_{\pm 0.22}(\Delta m_{15}-1.1)^3, \sigma = 0.043 \quad (1)$$

The dispersion of ∼0.04 mag is comparable to the intrinsic dispersion of the evolution of the "tail" color (e.g. Lira 1995, Phillips et al. 1999), and is much less than that of the peak color−Δm_{15} relation. The residual distribution for the fit to the color-Δm_{15} correlation, as shown in Figure 2, reveals that the larger scatter of the peak colors is not due to individual observations but tends to be an overall behavior.

Theoretically, the SN colors are related to the exact changes of the optical depth in the ejecta. The peak colors of SNe Ia show very rapid evolution and small measurement errors may result in systematically incorrect reddening measurements (Leibundgut 2001). For these reasons, we would prefer to use the post-maximum color ΔC_{12} as an alternative reddening

indicator. Remember that Equation (1) is derived from SNe Ia with $0.8 < \Delta m_{15} < 2.0$, and it may not apply to those SNe Ia with decline rates beyond the above range (e.g., SN 2001ay, which has the broadest light curve with $\Delta m_{15} = 0.69$; see Howell & Nugent 2003). Deviation of the observed ΔC_{12} from the curve shown in the bottom panel of Fig.1 gives an estimate of the host galaxy reddening $\mathrm{E}(B-V)_{12}$ which is listed in column (12) of Table 1. The above determinations of the host galaxy reddening are well consistent with those estimated by the color at the nebular epoch, with an offset of ∼0.01 mag and a dispersion of ∼0.04 mag.

The host galaxy reddening $\mathrm{E}(B-V)_{host}$ was taken to be the weighted average of $\mathrm{E}(B-V)_{12}$ and $\mathrm{E}(B-V)_{tail}$ (cf. Phillips et al. 1999, Altavilla et al. 2004). In some cases, the formal mean value turns out to be negative specifically, the $\mathrm{E}(B-V)_{host}$ values were assumed to be zero. This is equivalent to adopting a Bayesian filter with a flat prior distribution for positive $\mathrm{E}(B-V)$ and zero for $\mathrm{E}(B-V) < 0$ (Riess et al. 1996a). The adopted $\mathrm{E}(B-V)_{host}$ values are listed in column (13) of Table 1.

Figure 3 shows the distribution of the reddening $\mathrm{E}(B-V)_{host}$ in their host galaxies (see § 4.1 as a function of the normalized distance $\mathrm{r}_{SN}/\mathrm{r}_{25}$). The SNe further out are found to have lower reddening values than those in the inner regions. The mean $\mathrm{E}(B-V)_{host}$ value for the SNe in E/S0 galaxies is found to be 0.07±0.02 mag. Excluding the largest contributor SN 1986G in reddening, the mean reddening value still remains at a non-negligible level of ∼0.05 mag.

We further compared the values of the host galaxy reddening derived in this paper to the corresponding ones given in R05. As shown in the lower panel of Fig.3, the mean value of R05 appears to be lower than ours by 0.047±0.051 mag. This difference is related to the assumption on the reddening-free SN sample and the approach to estimate the host galaxy reddening. For example, we define a low-reddening sample of SNe Ia using a color cut of $\mathrm{E}(B-V)_{tail} \lesssim 0.06$ mag, while R05 assumed that all SNe in E/S0 galaxies are free from reddening. According to our analysis, however, the SNe in the E/S0 galaxies may not necessarily guarantee a reddening-free sample.

3.2. Empirical reddening relations

An understanding of the absorptions relies not only on the availability of independent reddening indicators but also on the knowledge of the dust properties. The determination of R for the reddening ratios from SNe Ia implies astonishingly different optical properties for dust in distant galaxies. Earlier analysis assuming that SNe Ia have a unique luminosity and color yielded surprising smaller values of $R_B \sim 1.0-2.0$ (e.g. Branch & Tammann 1992).

Recent determinations of R tend to give more consistent values, e.g. $R_B = 3.55\pm 0.30$ (Riess et al. 1996b), 3.5±0.4 (Phillips et al. 1999), 3.5 (Altavilla et al. 2004), and 3.65±0.16 (Reindl et al. 2005). The slight variations among these values are related to the ways of deriving the host galaxy reddening for SNe Ia.

To examine the dust properties of distant galaxies using SNe Ia, it is important to first remove the intrinsic dependence of SN Ia luminosity on the light or color curve parameters. We have shown in Fig.3 of W05 that the peak luminosities of SNe Ia with minimum absorption can be well calibrated by the color parameter ΔC_{12}. The relation between ΔC_{12} and the absolute magnitudes M in $UBVI$ (which were obtained by assuming $H_0 = 72$ km s^{-1} Mpc^{-1}), based on a sample of 33 Hubble flow SNe Ia with $E(B-V)_{host} \lesssim 0.06$ mag as listed in Table 1 (including four 91T/99aa-like objects, four 91bg-like objects and SN 2001ay), can be expressed in terms of linear relations:

$$M_U = -19.75_{\pm 0.09} + 2.55_{\pm 0.15}(\Delta C_{12} - 0.31), N = 10, \sigma = 0.202 \quad (2)$$

$$M_B = -19.30_{\pm 0.02} + 1.93_{\pm 0.07}(\Delta C_{12} - 0.31), N = 33, \sigma = 0.108 \quad (3)$$

$$M_V = -19.24_{\pm 0.02} + 1.43_{\pm 0.06}(\Delta C_{12} - 0.31), N = 33, \sigma = 0.097 \quad (4)$$

$$M_I = -18.97_{\pm 0.02} + 1.01_{\pm 0.06}(\Delta C_{12} - 0.31), N = 30, \sigma = 0.101 \quad (5)$$

The normalization to $\Delta C_{12} = 0.31$ corresponds to the color value of the fiducial supernova 1992al. The dispersion of the $M - \Delta C_{12}$ relation for 24 normal SNe Ia with low dust reddening decreases further down to 0.170 mag in the U band, to 0.069 mag in B band, to 0.068 mag in V band, and to 0.069 mag in I band, respectively. And the corresponding slopes in $UBVI$ are 1.97±0.52, 1.72±0.11, 1.41±0.10, and 0.96±0.10, respectively, which are not inconsistent with those shown in the above equations. This demonstrates the robustness of the correlation between the post-maximum color ΔC_{12} and the absolute magnitudes M, in particular in the V and I bands. The larger dispersion in the U band may be caused by small number statistics, the intrinsically larger luminosity dispersion as suggested by Jha et al. (2006a), or both of them.

The ΔC_{12} procedure thus provides an independent and more precise way to determine the average value of the reddening ratio for distant galaxies hosting SNe Ia. The absolute magnitudes M_{UBVI} of all 109 SNe Ia, corrected for the Galactic extinction and the intrinsic dependence on ΔC_{12} as shown by Eqs.(2)-(5), are plotted against the values of their host galaxy reddening in Figure 4.

SNe shown in Figure 4 with $v \lesssim 3{,}000$ km s^{-1} (represented by open squares) were not used for the fit of the reddening vector due to the effect of the peculiar motions of their host galaxies. Moreover, the two Hubble flow events SNe 1999ej and 2002cx were also not

included in the fit. The former is too faint for unknown reasons by about 0.6 mag for a normal supernova. The latter is characterized by a 1991T-like pre-maximum spectrum and a 1991bg-like luminosity, a normal $B-V$ color evolution, and very low expansion velocities (Li et al. 2003), which may be a new subclass of SNe Ia (Jha et al. 2006b). For the linear fits in Figure 4, the resulting values of R_{UBVI} are:

$$R_U = 4.36 \pm 0.25, R_B = 3.33 \pm 0.11, R_V = 2.29 \pm 0.11, R_I = 1.18 \pm 0.11 \quad (6)$$

which are clearly smaller than the standard values for the Milky Way. Our determinations of the R values are slightly lower than most of the recent determinations. From a sample of 62 Hubble flow SNe Ia, Reindl et al. (2005) reported recently a value of R_B=3.65±0.16. Although there were a lot of the same SNe in our analysis, the host galaxy reddening E$(B-V)_{host}$ we derived for these SNe was different (see §3.2). The smaller reddening values obtained by Reindl et al. consequently led them to derive the larger R value. Note that they also derived their E$(B-V)_{host}$ values from the peak $V-I$ colors, which usually have larger scatter (e.g., 0.08-0.09 mag) and may be not so reliable as a reddening indicator. Very recently, Wang L et al. (2005) determined a lower value of $R_B = 2.59 \pm 0.24$ from a combining analysis of the maximum luminosity and the luminosity at CMAGIC region. This value may parameterize well the effects both of extinction by host galaxy and of intrinsic SN color dependence on luminosity, but not necessarily the true R value for distant galaxies since they did not try to disentangle these two effects in the analysis. Moreover, their analysis did not include two of the most highly reddened SNe 1995E and 1999gd in the Hubble flow, which may have significant impact on the final R values.

The remarkably small scatter associated with the above R_{UBVI} values indicates that the host galaxies for most of the SNe Ia within $z \lesssim 0.1$ do share fairly similar dust properties. Besides the two Hubble flow SNe mentioned above, the highly reddened SN 1999cl (not shown in Figure 4) is likely to be an outlier, which deviates from the best fit line by ∼1.1 mag in B band. The disturbance of the peculiar motion cannot account for the large deviation of SN 1999cl since its host galaxy NGC 4501 (M88) is the member galaxy of the Virgo cluster. Assuming an average luminosity and a peculiar motion of $\lesssim$200 km s^{-1} for SN 1999cl, one finds $R_B = 2.40 \pm 0.37$ for this individual supernova. This indicates M88 may have a very non-standard dust (see also Krisciunas et al. 2005 for an argument of a low R_V ∼1.55 for SN 1999cl). SN 1997br also seems to be an outlier, which was a spectroscopically peculiar, 91T-like object (Li et al. 1999). Applying our R values to correcting the host galaxy extinction of SN 1997br would make it be unrealistically bright, in particular in the U band where it is brighter than a normal SN Ia by ∼1.2 mag. This difference probably suggests a very different dust property for the host galaxy of SN 1997br, ESO 576-G40. However, there is still a large uncertainty in the measurement of the recession velocity of ESO 576-G40 (see discussions in Li et al. 1999), which may also contribute in part to the large deviation of

SN 1997br as seen in Fig.4. For the normal and low-reddening SN 2003du (Anupama et al. 2005), a peculiar motion of ∼800 km s^{-1} relative to the the CMB frame, is needed to explain its "outlying position" in Fig.4.

4. The Luminosity Properties of SNe Ia

Estimates of the host galaxy reddening and determinations of the empirical reddening relations, based on a larger SN Ia sample of different sorts, would enable us to de-redden SNe Ia accordingly. This will consequently help to reveal the nature of SNe Ia and to determine the relevant parameters governing their optical properties.

4.1. The luminosity diversities

In Figure 5, we plot the distribution of the extinction-corrected absolute magnitudes in $UBVI$ with a bin size of 0.2 mag for all 109 SNe listed in Table 1.

As known in previous studies, different SNe Ia span a wider range over their optical properties (e.g., see Leibundgut 2001 for a review). It is clear from Fig.5 that both the maximum value and the scatter of the luminosity are wavelength-dependent. Compared with the luminosity of SNe Ia in the I band, the luminosity in the U band is more luminous and the scatter is also larger. This can be interpreted as that the SN Ia emission in the U band may be more sensitive to the variance of the progenitor properties, such as the metallicity (Hoeflich et al. 1998; Lentz et al. 2000).

The spectroscopically peculiar, 91T-like and 99aa-like events lie at the brighter end of the luminosity distribution of SNe Ia, which are ∼0.3 mag brighter than the normal SNe Ia (Branch et al. 1993). Moreover, these overluminous events seem to have relatively uniform peak luminosity, with a small scatter of about 0.13 mag in the BVI and 0.20 mag in the U band. On the other hand, the faintest SNe Ia are almost characterized by the 91bg-like events but for the most peculiar SN 2002cx. In the contrary to the 91T/99aa-like SNe Ia, the 91bg-like events cover a wider range of peak luminosities from ∼2 mag to ∼0.6 mag in different wave bands. The luminosity distributions of SNe Ia in $UBVI$ bands can be roughly fitted by Gaussians. The long tail at the faint end indicates a continuous distribution of the peak luminosities between the Branch-normal SNe Ia and the 91bg-like events, possibly suggesting a common origin for their progenitors.

4.2. The environmental effects on SN Ia luminosity

Locations of the SNe Ia in their host galaxies may offer clues to understand the origin of SN Ia optical diversities (e.g., Wang et al. 1997), as the properties of the stellar populations [e.g., metallicity and age] may vary from galaxy to galaxy and vary with the spatial positions within a galaxy. In Figure 6, we show the radial distribution of the absolute magnitudes M_V, corrected for the absorption in the Galaxy and the host galaxy as laid out in §3. The SN location (here we only considered the radial position) is defined as the relative galactocentric distance r_{SN}/r_{25}, where r_{SN} is the de-projected radial distance of the SNe Ia from the galactic center, and r_{25} is the de Vaucouleurs radius of that galaxy (e.g., de Vaucouleurs 1991).

To examine the age effect on SN Ia luminosity, we treat SNe in late-types (spiral galaxies) and early-types (S0 and elliptical galaxies) separately, where the stellar populations are assumed to be different. We find that SN Ia luminosity is related to the morphological types of the host galaxies. Brighter SNe Ia tend to occur in spiral galaxies with younger stellar populations, while most of the fainter events occur preferentially in the E/S0 galaxies with relatively older stars. This dichotomy was first noticed by Hamuy et al. (1996c), and was later confirmed by Riess et al. (1999) and Hamuy et al. (2000). This observational fact argues for the age difference in the progenitors as the origin of SN Ia optical diversities. Nevertheless, such an age effect alone seems unlikely to account for the occurrence of the brighter object SN 1998es (with $\Delta m_{15} = 0.87$) in the lenticular galaxy NGC 632 and the presence of the fainter event SN 1999by (with $\Delta m_{15} = 1.90$) in the Sb galaxy NGC 2841.

On the other hand, we did not find any radial variation for SN Ia luminosity in spiral galaxies alone, which is consistent with previous studies (Parodi et al. 2000; Ivanov et al. 2000). The SNe in E/S0 galaxies (represented by open circles) at the first glance do not show any significant correlation between the luminosity and the radial position r_{SN}/r_{25}. Omitting arbitrarily those peculiar SNe Ia, e.g. the 91bg-like events as labelled in Fig.5, however, a trend with the galactocentric distances seems to emerge for the others. A radial gradient of 0.30 ± 0.12 was found for normal SNe Ia in E/S0 galaxies, which is significant at a confidence level of $\sim 2.5\sigma$.

If the magnitude gradient observed for normal SNe Ia in E/S0 galaxies was true, then the radial metallicity variation in elliptical galaxy (Henry & Worthey 1999) may be responsible for the diversities of SN Ia luminosities because the stellar populations in these earlier galaxies are generally believed to be coeval (Worthey 1994; Vazdekis et al. 1997). Theoretically, the metallicity effect on the range of SN Ia luminosity may be understood by the "strong wind" models proposed by Umeda et al. (1999) who suggests that the lower-metallicity systems will tend to have larger initial C/O masses and hence produce fainter SNe Ia. The lack of magnitude gradient in spiral galaxies may be the counteracting result from the effects both

of age and metallicity since the stellar populations in the inner regions of spiral galaxies are, in general, both more metal rich and older in relation to those in the outer regions (Henry & Worthey 1999). In order to further disentangle these two environmental aspects, one may need to resort to the spectroscopic studies of SN Ia host galaxies as suggested by Hamuy et al. (2000).

4.3. Luminosity dependence of SNe Ia on the secondary parameters

The correlations between SN Ia peak luminosities and the secondary parameters were specifically investigated by Parodi et al. (2000) and have recently been revisited by Reindl et al. (2005). Their studies suggested that the decline rate Δm_{15} and the peak $B-V$ color (see also Tripp 1998; Tripp & Branch 1999) are the two key parameters for the homogenization of SN Ia luminosities. To examine this relationship, the absorption-corrected absolute magnitudes M_V of 73 Hubble flow SNe (see the definition in §5.1) are thus plotted against the decline rate Δm_{15}, the peak $B-V$ color, as well as the post-maximum color ΔC_{12} in Figure 7. The 11 nearby SNe Ia with cepheid distance calibrations from Table 5 are also overlaid in the figure.

The dependence of SN Ia peak luminosity on the decline rate Δm_{15} becomes apparently nonlinear for the full SN sample with different spectral types as shown in Fig.7a (the left panel of Fig.7). Excluding SN 2001ay, however, a cubic spline seems to give a perfect fit to the $M_V - \Delta m_{15}$ relation with a dispersion of $\sim$0.12 mag. The cubic polynomial dependence and the small dispersion are expected if the color term ΔC_{12} in Eq.(4) is substituted by the right side of Eq.(1).

Fig.7b shows the $M_V - (B_{max} - V_{max})$ plot. Although the peak color $B_{max} - V_{max}$ connects well with fainter SNe Ia at the redder end, it is very loosely related to the peak luminosity for most of the SNe Ia with $-0.1 \lesssim B_{max} - V_{max} \lesssim 0.1$ mag. The linear fit yields a larger dispersion of $\sim$0.23 mag for the points in Fig.7b, which indicates that the peak color alone cannot delineate the peak luminosity of SNe Ia. Combining both Δm_{15} and $B_{max} - V_{max}$ in the homogenization can reduce the luminosity dispersion to $\sim$0.16 mag, which is consistent with what obtained by R05.

The correlation of the extinction-corrected absolute magnitudes with ΔC_{12} is illustrated in Fig 7c. As it can be seen, the tight and linear $M_V - \Delta C_{12}$ relation found for the reddening-free SNe still holds well for the larger SN sample. The rms scatter yields along the best fit line is $\lesssim$0.12 mag in BVI, which corresponds to a distance uncertainty of 5-6%. As the host galaxy reddening $\mathrm{E}(B-V)_{host}$ was also partially derived from the observed color ΔC_{12},

it is necessary to examine the possible interplay of these two variables. The corresponding regression with these two variables takes the form of

$$M_{UBVI} = b_{UBVI}(\Delta C_{12} - E(B-V)_{host} - 0.31) + R_{UBVI}E(B-V)_{host} + M^0_{UBVI} \quad (7)$$

leading further to

$$M_{UBVI} = b_{UBVI}(\Delta C_{12} - 0.31) + (R_{UBVI} - b_{UBVI})E(B-V)_{host} + M^0_{UBVI} \quad (8)$$

where the constant term, M^0_{UBVI}, is the mean absolute magnitude reduced to $\Delta C_{12} = 0.31$. Least-squares solutions for all 73 Hubble flow SNe in Fig.7 give the values of b_{UBVI}, R_{UBVI}, and M^0_{UBVI} as shown in Table 3. The improved R_{UBVI} values are very close to the provisional values determined from Fig.4, and the slopes of the correlation b_{UBVI} agree quite well with those shown in Eqs.(2)-(5). This suggests that the two variables $\mathrm{E}(B-V)_{host}$ and ΔC_{12} are quite independent of each other. Note that the slope of the correlation and the reddening ratio show very similar values in the I band. In other words, we can homogenize well the $I-$band luminosity of SNe Ia by the single parameter ΔC_{12} without knowing the host galaxy reddening (because the second term of the right side of Eq.(8) approximately drops out).

The small dispersion given by the $M-\Delta C_{12}$ relation (see Table 3 and Fig.7) leaves little room for the dependence of SN Ia luminosity on other secondary parameters. To further strengthen our case, we examine the remaining dependence of the $M_V-\Delta C_{12}$ relation fits on other secondary parameters (see Figure 8). After homogenization as to ΔC_{12} according to Eq.(7), the magnitude residuals $\delta \mathrm{M}_V$ from the best fit in Fig.7c did not show any significant dependence on the decline rate Δm_{15}, or on the peak $B-V$ color. As it can be seen from Fig.8, the luminosity gradient with the galactocentric distances $\mathrm{r}_{SN}/\mathrm{r}_{25}$ found for SNe Ia in E/S0 galaxies also becomes marginally important with a confidence level of $\lesssim 1\sigma$. This shows that the environmental effects (such as the metallicity and /or the age of the progenitors) on SN peak luminosity can be removed or substantially reduced via ΔC_{12} calibration.

The $M-\Delta C_{12}$ relation is re-examined and confirmed for a larger SN sample, which allows us to calibrate SNe Ia using ΔC_{12} with more confidence. It should be emphasized that this is still not a universal relation, as there are still extremely "anomalous" or rare events, such as SN 2002cx which cannot be calibrated by any known methods.

5. The distance scales

5.1. The Hubble diagram of SNe Ia

An effective way of assessing the quality of SNe Ia as distance indicators is to plot them in the Hubble diagram. The two quantities entering the Hubble diagram − magnitude

m and redshift $z-$ are direct tracers for the expansion history of the Universe. Our data sample consists of 109 well-observed SNe Ia; nevertheless, not all of them are suitable for constructing the Hubble diagram and exploring the expansion rate of the Universe. We have intentionally excluded those SNe Ia in galaxies with $cz \lesssim 3{,}000$ km s^{-1} to reduce the uncertainties from the peculiar motions. In addition, we further excluded SN 1996ab with $cz = 37370$ km s^{-1}, where the cosmological effect on the luminosity distance becomes important (Jha et al. 1999). After these selections, the remaining sample consists of 73 SNe Ia in the Hubble flow.

At distances of z$\lesssim$0.1, the dimming of a standard candle as function of redshift z can be simply described by

$$m = 5logcz + \alpha, \tag{9}$$

where cz is the recession velocity corrected to the CMB frame, and α is the "intercept of the ridge line" given by

$$\alpha = 5logH_0 - M - 25. \tag{10}$$

It follows immediately that

$$H_0 = 10^{0.2(M\ +\ \alpha\ +\ 25)}. \tag{11}$$

By Equation (11), determination of the Hubble constant H_0 from SNe requires their absolute magnitudes and the intercept of their Hubble lines. The absolute magnitudes are obtained by observations of nearby SNe Ia with Cepheid distances (see §5.2), while the intercept α can be determined by observations of the Hubble flow ones.

In Figure 9, we present the $U-$, $B-$, $V-$, and $I-$band Hubble diagrams (or $m - z$ relation) for the 73 Hubble flow SNe Ia. The apparent magnitudes are corrected for the ΔC_{12} dependence and the host galaxy absorption according to Eq.(7). The small scatter in the Hubble diagram results in precise determination of the α value in Eq.(9), which are -4.18 ± 0.03 in U, -3.64 ± 0.01 in B, -3.56 ± 0.01 in V, and -3.25 ± 0.01 in I, respectively. To test the robustness of the global fit, we examined the $m - z$ relation using different subsets of SN sample in the Hubble flow. This includes the recession velocity, the host galaxy reddening, and the spectral types of SNe Ia. The best fit results are summarized in Table 4. Note that the number shown in column (2) of Table 2 refers to the SN number with available data in the B and V bands.

The Hubble lines defined by SNe Ia with different spectral types (e.g., normal, 91T/99aa-like, and 91bg-like) may have remarkable offsets in the zeropoints, due to the larger difference between their intrinsic luminosities (see Fig. 5). As a test of the spectral dependence, we examined the Hubble diagrams constructed by normal, 91T/99aa-like, and 91bg-like SNe Ia, respectively. It turns out that the α values derived from the peculiar SNe Ia are consistent

with the global fit within ±0.15 mag (see Table 4). Including a fraction of ∼20% peculiar events in the full SN sample appears not to affect the Hubble line. This is demonstrated by the statistically insignificant variations in the α values between the full sample and the sample of 58 normal ones.

As the normal SNe Ia look more uniform, with a small scatter of about 0.10 mag in $UBVI$ bands, they are appropriately used to probe the possible variation in the expansion rate. Zehavi et al. (1998) suggested a dynamic glitch in the Hubble diagram of SNe Ia at cz = 7,000 km s^{-1}, across which the expansion rate of the local Universe may change by a few percent. To examine this effect and the possible variation in α, we divided the sample of 58 normal SNe Ia into two subsample using the velocity cut at 7,000 km s^{-1}. The variations of the α values between the more distant SNe Ia and the nearby ones are found to be around 0.03 mag in BVI bands, which would lead to a discrepancy in the expansion rate less than 2%. The larger difference shown in the U band is more likely due to a statistical fluke since there are only 7 SNe Ia with U-band photometry beyond v = 7,000 km s^{-1}. However, more Hubble flow SN Ia sample and various analysis techniques are still needed to further diagnose the possible discontinuity of the expansion rate at the local Universe.

To explore the effect of the absorption corrections on the Hubble line, we considered the cases with restrictions on the maximum value of $E(B-V)_{host}$ in the fitting. Excluding the highly reddened SNe [i.e., $E(B-V)_{host} > 0.15$ mag], or even the SNe with $E(B-V)_{host} > 0.06$ mag from the Hubble diagram, the change in the α value is $\lesssim$0.02 mag in each waveband. This argues in favor of the self-consistent determinations of the host galaxy reddening and the unconventional R_{UBVI} values. Assuming the scatters shown by the fit to SNe Ia with minimum absorption [e.g., $E(B-V)_{host} \leq 0.06$ mag] as the intrinsic ones, we can estimate the uncertainties caused by the absorption corrections. By comparing them with those values shown in the fit of all normal SNe Ia, we place a limit on the errors of the absorption corrections as ∼0.08, 0.07, and 0.06 mag in B, V, and I bands, respectively. This is slightly smaller than the corresponding values derived from the errors of the host galaxy reddening given in Table 1. The small number of statistic sample prevented us from giving a reasonable value in the U band.

It is satisfactory that the Hubble flow SNe Ia of different subsets yield the same α values in each waveband within the errors, showing the robustness of the ΔC_{12} method. In particular, the dispersion around the Hubble line is impressively small for each subset of SN sample. For example, the dispersion for the sample of 58 normal SNe Ia is only 0.09-0.11 mag in full optical bands, corresponding to a ∼5% relative distance uncertainty per supernova[1].

[1]Considering the typical uncertainties of the redshift due to peculiar velocity (e.g. 300 km s^{-1} adopted

For comparison, the MLCS method yields $\sigma_B = 0.22$ mag for their gold sample of 67 SNe Ia (Riess et al. 2004), whereas the BATM calibration yields $\sigma_B = 0.21$ mag (BATM; Tonry et al. 2003). The two-parameter method (which involves both Δm_{15} and peak $B - V$ color corrections) revisited recently by Reindl et al. (2005) gives a dispersion of 0.16 mag for 63 SNe Ia. In an approximately parallel analysis, Wang L et al. (2005) obtained an rms scatter of $\sigma_B \approx 0.14$ mag for 33 selected SN sample. The SALT method (Guy et al. 2005) gives $\sigma_B = 0.16$ mag for a sample of 23 SNe Ia. In reference to above calibration methods, the ΔC_{12} method improves remarkably the distance accuracy from SNe Ia. This will invoke hopefully more precise determinations of the Hubble constant H_0 and other cosmological parameters. The application of the ΔC_{12} method to the Supernova Legacy Survey data (Astier et al. 2006) will be presented in a forthcoming paper.

5.2. Calibrations of the absolute magnitudes of SNe Ia

In order to infer the Hubble constant H_0, it is necessary to tie our ΔC_{12} distances to the SNe Ia with absolute magnitude calibrations. Cepheid variables, presently, through their Period-Luminosity ($P - L$) relation, are the fundamental primary distance indicators. We can thus establish the absolute magnitudes of SNe Ia through the distances measured from the Cepheid variables in their host galaxies.

Thanks primarily to the valuable contribution of the Saha-Tammann-Sandage SN Ia HST Calibration Project (hereafter STS), the number of SNe Ia with Cepheid distances to their host galaxies increased to thirteen so far. The STS consortium provided the Cepheid distances to SNe 1895B (NGC 5253), 1937C (IC 4182), 1972E (NGC 5253), 1981B (NGC 4536), 1960F (NGC 4496A), 1990N (NGC 4639), 1989B (NGC 3627), 1998aq (NGC 3982) and 1991T (NGC 4527) (Saha et al. 1996, 1997, 1999, 2001a, 2001b). The Cepheid distances to SN 1974G in NGC 4414, SN 1998bu in NGC 3368, and SN 1999by in NGC 2841 was obtained by Turner (1998), Tanvir et al. (1999), and Macri et al. (2001), respectively. Using the Advanced Camera for Surveys (ACS) on HST, Riess et al. (2005) recently measured the Cepheid distance to the more distant SN 1994ae in NGC 3370. These SNe Ia with Cepheid distances will provide the calibration for the absolute magnitudes of SNe Ia.

Nevertheless, analysis of the preceding Cepheid data does not reach a consistent result on the absolute calibration for SN Ia peak luminosity (see also discussions by Riess et al. 2005). Compared with the results of STS, the distances reanalyzed by HST key project

---

in our analysis), the actual uncertainty intrinsic to our ΔC_{12} distance calibration is less than 4%, which can be fully interpreted as the photometric errors.

(hereafter KP) are on average shorter by 0.2−0.3 mag (Gibson et al. 2000; Freedman et al. 2001). This discrepancy may arise primarily from the sample selection of the Cepheid variables and the choice of the $P-L$ relation (i.e., Saha et al. 2001a). The STS consortium used the earlier $P-L$ relation that was established by Madore & Freedman (1991; hereafter MF91), while the KP group employed a new $P-L$ relation which is based on the Cepheid data of the Optical Gravitational Lensing Experiment (OGLE) survey (Udalski 1999). The OGLE $P-L$ relation, with a flatter color-period relation of $(V-I) \propto 0.2\log P$, yields a shorter Cepheid distance by about 8% than that derived from the earlier MF91 relation. We preferred the OGLE-based $P-L$ relation and the resulting Cepheid distances (i.e., the KP distances; Freedman et al. 2001) in this paper, due to the well-sampled light curves and the accurate photometry of the OGLE Cepheids (Udalski et al. 1999; Sebo et al. 2002).

The Cepheid $P-L$ relation derived from LMC was traditionally considered to be universal for all other galaxies. However, there is increasing evidence for a significant dependence of the Cepheid properties on the metallicity of the host stellar populations. An empirical test of this dependence by Kennicutt et al. (1998) yielded $\Delta\mu_0\ /\Delta[\mathrm{O/H}] = -0.24\pm0.16$ mag dex^{-1}. Such a dependence is in agreement with the theoretical predictions by Fiorentino et al. (2002). Using a larger sample of 17 Cepheid hosts with independent distances, Sakai et al. (2004) obtained a more robust empirical correction relation $\Delta\mu_0\ /\Delta[\mathrm{O/H}] = -0.24\pm0.05$ mag dex^{-1} with reduced errors, which is adopted here as metallicity correction for the Cepheid distances.

Table 5 contains a list of partial parameters for 11 nearby SNe Ia with Cepheid distances (see Table 1 for other parameters in more details). The two historical SNe 1895 and 1960F were not included because their V light curves are unavailable to infer the ΔC_{12} value, and hence the host galaxy reddening. The KP distance moduli of these calibrators, with and without the metallicity corrections, are given in columns (3) and (4). The apparent V magnitudes (corrected for the Galactic absorption), the color parameter ΔC_{12}, and the host galaxy reddening are listed in columns (5)-(7). The fiducial magnitudes m^0_V, corrected for absorption and ΔC_{12} using Eq.(8), are given in column (8). The final absolute magnitudes of the calibrators, M^0_U, M^0_B, M^0_V, and M^0_I contained in columns (9)-(12), respectively, are derived by subtracting the distance moduli $\mu_{KP}(\mathrm{Z})$ from the corresponding apparent magnitudes m^0_{UBVI} (here we only listed in Table 5 the case for apparent V magnitudes for the space limit). The uncertainties associated with the absolute magnitudes for each calibrator were obtained by combining in quadrature the quoted errors δm, $\delta\Delta C_{12}$, $\delta\mathrm{E}(B-V)_{host}$, and $\delta\mu_{KP}(Z)$.

The weighted average of the peak absolute magnitudes in $UBVI$ for the 11 nearby calibrators, reduced to $\Delta C_{12} = 0.31$ using Eq.(8) and the coefficients listed in Table 3, are

given as

$$M_U = -19.89 \pm 0.08 \text{ mag},\ \sigma_U = 0.14 \text{ mag} \quad (12)$$

$$M_B = -19.33 \pm 0.06 \text{ mag},\ \sigma_B = 0.11 \text{ mag} \quad (13)$$

$$M_V = -19.27 \pm 0.05 \text{ mag},\ \sigma_V = 0.11 \text{ mag} \quad (14)$$

$$M_I = -18.97 \pm 0.04 \text{ mag},\ \sigma_I = 0.08 \text{ mag} \quad (15)$$

Excluding the spectroscopically peculiar SNe 1991T and 1999by, or further dropping the highly reddened SNe 1989B and 1998bu in the analysis, the change in the mean value of the absolute magnitudes at maximum is minor (i.e., $\lesssim$0.03 mag). If the metallicity effect was not taken into account, the distances to SN Ia host galaxies and consequently the peak luminosity of SNe Ia would be underestimated by $\sim$0.1 mag. Meanwhile, the scatter of the mean absolute magnitudes would increase significantly, i.e. from $\sim$0.11 mag to 0.16 mag in the V band. This also argues in favor of the metallicity correction of the Cepheid distances purely by virtues of reducing the luminosity dispersion of the SN calibrators

Inspection of the M^0 values listed in Table 3 shows that the Hubble flow SNe Ia have approximately the same absolute magnitudes as the more nearby ones calibrated via Cepheids. This fact suggests that the value of H_0 (72 km s^{-1} Mpc^{-1}), assumed for determining the distances to the SNe in the Hubble flow, must have been very close to the H_0 value implied from the KP Cepheid distances. This similarity is not a foregone consclusion but results from a coincidence. If we take the distance moduli from STS to calibrate SNe Ia, however, the predicted absolute magnitudes of SNe Ia would increase by $\sim$0.25 mag, i.e., $M_B = -19.58 \pm 0.06$ and $M_V = -19.51 \pm 0.05$ mag, which will lead to a Hubble constant lower than the assumed value.

Combinations of the peak absolute magnitudes M^{corr}_{UBVI} shown in Eqs. (12)-(15) with the individual apparent magnitudes m^{corr}_{UBVI} of 109 SNe Ia can give the luminosity distances to 109 SNe Ia [Table 2, columns (6)-(9)]. The luminosity distances, especially those in the U band, are important for comparison between the cosmological distances of SNe Ia beyond z$\geq$0.8. The distance moduli presented in Table 2 can also be used to constrain the peculiar motions of the nearby galaxies hosting SNe Ia.

5.3. Determination of the Hubble constant H_0

Taking the zero-points of the Hubble lines from Table 4 and inserting the absolute magnitudes of the SN calibrators into Eq.(11), we can obtain the value for the Hubble constant H_0. The key results for five different combinations of the Hubble flow SNe Ia and the nearby calibrators are summarized in Table 6.

For all of the Hubble flow SNe (N = 73) and the nearby calibrators (N = 11), the combination yields consistent determinations of $H_0 = 72\pm2$ in the B, V, and I bands; the smaller value yielded in the U band may be due to the statistical fluctuation. Omitting 14 peculiar SNe from the Hubble flow and 2 from the nearby calibrators, the similar procedure reproduced well the $H_0(U, B, V, I)$ values for the full sample. By further eliminating the highly reddened SNe [i.e., those with $E(B-V)_{host} > 0.15$ mag], one finds similar $H_0(U, B, V, I)$ values from the remaining sample (47+7). We also examined the extreme case for the spectroscopically peculiar SNe Ia. For 91T/99aa-like SNe Ia, the resulting H_0 value is 68±3, while the 91bg-like events give a value of 75±5. It is reassuring that both the normal SNe Ia and the peculiar ones yield consistent determinations of the Hubble constant within the errors.

In all of the above five cases, the weighted mean value of H_0 is within $68 \leq H_0 \leq 75$. This suggests that our results are not sensitive to different subsets of SNe Ia, and that no obvious systematic errors are being introduced by absorption corrections or including the peculiar SNe in the analysis. Taking the former three cases shown in Table 6 as the most consistent determinations, a value of 72±1 is obtained for the Hubble constant. Restricting the analysis to the four best calibrators of SNe 1981B, 1990N, 1994ae, and 1998aq as ranked by Riess et al (2005), the resulting H_0 value remains almost unchanged. Taking into account the intrinsic luminosity dispersion implied from the Hubble flow SNe Ia, e.g., $\lesssim$0.12 mag in BVI bands, the H_0 value becomes as

$$H_0 = 72 \pm 4(statistical) kms^{-1}Mpc^{-1} \tag{16}$$

The uncertainty accounts for the statistical error of the absolute magnitude calibration of nearby calibrators and the dispersion in the Hubble diagram of Hubble flow SNe Ia.

In accord with Riess et al. (2005), especially their Table 13 (but also see Freedman et al. 2001 for more detailed discussions of the systematic error budget), two main sources of error were incorporated into the systematic error budget. Uncertainties in the LMC zero point enters at a level of 0.10 mag and the slope of the $P-L$ relation is at a level of 0.05 mag. In quadrature, the overall systematic error budget amounts to 0.11 mag, corresponding to about 6% in H_0. In combination with the statistical error and the systematic error, the final result for the Hubble constant yields

$$H_0 = 72 \pm 4(statistical) \pm 4(systematic) = 72 \pm 6(total) kms^{-1}Mpc^{-1} \tag{17}$$

This H_0 value, based on the homogenization of the ΔC_{12} method, is in excellent agreement with that determined by the MLCS2k2 method (Riess et al. 2005), and is also fully consistent with the determinations from the Wilkinson Microwave Anisotropy Probe (WMAP) data (Spergel et al. 2003). However, the true uncertainty in our value of the Hubble constant

may indeed be somewhat larger than our formal value due to the controversial Cepheid distances to the SN Ia host galaxies (e.g., Saha et al. 2006).

6. Discussion and Conclusions

A larger sample of 109 SNe Ia has been compiled from the literature to investigate the properties of the dust in their host galaxies. Using the host galaxy reddening derived from ΔC_{12} and the tail colors of SNe Ia, we found smaller values for the reddening ratios of R_U = 4.37±0.25, R_B = 3.33±0.11, R_V =2.30±0.11, and R_I = 1.18±0.11, which are smaller than the standard R_{UBVI} values of 5.5, 4.3, 3.3, and 1.8, respectively. The drastic explosion of the SNe may in some manner change the distribution or properties of the dust grains surrounding the pre-supernova. Another possible explanation for the observed lower values of R turns to the dust in the circumstellar environment of SNe (Wang 2005), which may be substantially different from the interstellar dust.

In particular, we have discussed the luminosity dependence on the environmental parameters, such as the morphological type of the host galaxy and the location of the SNe within the galaxy. As first noted by Hamuy et al. (2000) and also confirmed by our study, the brighter SNe prefer to occurring in the late-type (spiral) galaxies and the fainter ones prefer to occurring in the early-type (E/S0) galaxies. However, there are two counter examples: one is SN 1998es, which was a 91T-like event and exploded in the lenticular galaxy NGC 632; the other is SN 1999by, which was a 91bg-like event and occurred in the Sb−type galaxy NGC 2841. These two cases suggest that the age may not be an exclusive factor underlying SN Ia diversities. The radial gradient of the absolute magnitudes (at a confidence of $\sim 2.5\sigma$) found for normal SNe Ia in E/S0 galaxies implies that the metallicity is probably another important factor responsible for the range of SN Ia luminosities.

Using 73 Hubble flow SNe Ia, we also examined the correlations between SN Ia luminosities and the secondary parameters such as the decline rate Δm_{15}, the peak $B-V$ color, and the postmaximum color ΔC_{12}. We found that the relation between the peak luminosity and the light curve shapes becomes apparently nonlinear, and more complicated function is needed to describe this relationship. The correlation of the peak luminosity and the peak color shows a large scatter of ∼0.23 mag around the best fit line, which is not tight enough to get reliable calibrations for SNe Ia. Compared with Δm_{15} and $B_{max}-V_{max}$, the color parameter ΔC_{12} can depict extremely well the peak luminosity of SNe Ia, with an impressively small dispersion of $\lesssim$0.12 mag in BVI. One example to illustrate the superiority of ΔC_{12} calibration is SN 2001ay, which has a very broad light curve with $\Delta m_{15} = 0.69$ but a normal luminosity, i.e. $M_V = -19.0$ mag. If a Δm_{15} correction is applied, the magnitude would be

overcorrected by ∼0.8 mag, i.e. ∼−18.5 mag. Whereas the ΔC_{12} correction gives a more reasonable magnitude of −19.10 mag, much closer to the fiducial value: $M_V \approx -19.25$ for SN 1992al. Note that the ΔC_{12} method, at present, is still an officially empirical relation and more is needed to understand its underlying physics, e.g., the well-behaved opacity in the expanding fireball.

The Hubble diagrams in U, B, V, and I are displayed for 73 Hubble flow SNe Ia using the fully corrected apparent magnitudes. Solutions for the zeropoint α of the Hubble line are given for various subsets with different restrictions. We first inspected the velocity restriction. The Hubble diagram constructed by the two subsets, with different velocities demarcated at v = 7,000 km s^{-1} yet comparable sizes of SN sample, show little variation in α values and the scatters. Inspections of the reddening restriction suggests that the α values are also insensitive to the accepted maximum value of a host galaxy reddening. The uncertainties caused by the absorption correction were found to be $\lesssim$0.08 mag in BVI, which justifies the reliability of our adopted absorption correction for SNe Ia. We finally examined the effect of the peculiar SNe Ia on the Hubble line. After ΔC_{12} correction, the larger luminosity difference between the normal SNe Ia and the peculiar ones has been narrowed down to ±0.15 mag. Inclusion of a fraction of $\lesssim$20% peculiar SNe Ia in the Hubble diagram will not significantly change the Hubble line.

With Cepheid distances to 11 nearby SN Ia, including two peculiar ones SNe 1991T and 1999by, we have calibrated the absolute magnitudes of SNe Ia and found the fully corrected mean value: $M_U^0 = -19.89 \pm 0.08$, $M_B^0 = -19.33 \pm 0.06$, $M_V^0 = -19.27 \pm 0.05$, and $M_I^0 = -18.97 \pm 0.04$. The forthcoming observations of SN 2006X in M100 (NGC 4321, which has a Cepheid distance; see Freedman et al. 2001) will further improve the determinations of the absolute magnitudes of SNe Ia. Applying the above calibration value to the Hubble flow SNe Ia, we derived the Hubble constant to be 72 ± 6 (total) km s^{-1} Mpc^{-1}. This value seems to be more robust and does not change with various combinations of distant SNe Ia and nearby calibrators. Reducing the uncertainty in the Hubble constant relies on a better understanding of the Cepheid $P - L$ relation, the metallicity correction, and more importantly, a more precise estimate of the distance to the LMC.

This work has been supported by the National Science Foundation of China (grants 10303002), the Basic Research Foundation at Tsinghua University (JCqn2005036), and the National Key Basic Research Science Foundation (NKBRSF TG199075402). We thank the referee for a number of valuable comments and suggestions that helped us to improve the paper. We are grateful to Dr. Weidong Li for allowing us to use the data of SN 2002el before publication.

REFERENCES

Altavilla, G., et al. 2004, MNRAS, 349, 1344

Anupama, G. C., Sahu, D. K., Jose, J. 2005, A&A, 429, 667

Ardeberg A., & de Groot M. 1973, A&A, 28, 295

Astier, P., et al. 2006, A&A, 447, 31

Benetti, S., et al. 2004, MNRAS, 348, 261

Branch, D., & Tammann, G.A. 1992, ARA&A, 30, 359

Branch, D., Fisher, A., & Nugent, P. 1993, AJ, 106, 2383

Branch, D., Romanishin, W., & Barbon, E. 1996, ApJ, 465, 73

Branch, D. 1998, ARA&A, 36, 17

Candia, P., et al. 2003, PASP, 115, 277

Cristiani S., et al. 1992, A&A, 259, 63

de Vaucouleurs, G., et al. 1991., Third Catalogue of Bright Galaxies (New York: Springer)(RC3)

Fillipenko, A. V., et al. 1992a, ApJ, 384, L15

Fillipenko, A. V., et al. 1992b, AJ, 104, 1543

Fiorentino, G., Caputo, F., Marconi, M., Musella, I. 2002, ApJ, 576, 402

Freedman, W. L., et al. 2001, ApJ, 553, 47

Garnavich, P., et al. 2004, ApJ, 613, 1120

Gibson, B. K., et al. 2000, ApJ, 529, 723

Goldhaber, G., et al. 2001, ApJ, 558, 359

Guy, J., Astier, P., Nobili, S., Regnault, N., Pain, R. 2005, A&A, 443, 781

Hamuy, M., Phillips, M.M., Suntzeff, N.B., Schommer, R.A., Maza, J., & Aviles, R. 1996a, AJ, 112, 2398

Hamuy, M., et al. 1996b, AJ, 112, 2408

Hamuy, M., et al. 1996c, AJ, 112, 2391

Hamuy, M., Trager, S.C., Pinto, P.A., Phillips, M.M., Schommer, R.A., Ivanov, V., & Suntzeff, N.B. 2000, AJ, 120, 1479

Henry, R. B. C., & Worthey, G. 1999, PASP, 111, 919

Hoeflich, P., Wheeler, J. C., & Thielemann, F. K. 1998, ApJ, 495, 617

Howell, A, & Nugent, P. 2004 in Cosmic explosions in three dimensions: asymmetries in supernovae and gamma-ray bursts, ed. by P. Hoflich, P. Kumar and J. C. Wheeler(Cambridge, UK: Cambridge University Press), p151

Ivanov, V. D., Hamuy, M., & Pinto, P. 2000, ApJ, 542, 588

Jha, S., et al. 1999, ApJS, 125, 73

Jha, S. 2002, PhD thesis, Harvard University

Jha, S., et al. 2006a, AJ, 131, 527

Jha, S., et al. 2006b, astro-ph/0602250

Knop, R.A., et al. 2003, ApJ, 598, 102

Kennicutt, R., et al. 1998, ApJ, 498, 181

Krisciunas, K., et al. 2001, AJ, 122, 1616

Krisciunas, K., et al. 2003, AJ, 125, 166

Krisciunas, K., et al. 2004a, AJ, 127, 1664

Krisciunas, K., et al. 2004b, AJ, 128, 3034

Krisciunas, K, et al. 2005, AJ, in press (astro-ph/0511162)

Madore, B. F., & Freedman, W. L. 1991, PASP, 103, 933

Modjaz, M., et al. 2001, PASP, 113, 308

Misra K., Kamble A. P., Bhattacharya, D. B., & Sagar, R. 2005, MNRAS, 360, 662

Leibundgut B., et al. 1993, AJ, 105, 301

Leibundgt B. 2001, A&AR, 10, 179

Lentz E. J., Baron, E., Branch, D., Hauschildt, P. H., Nugent, P. E. 2000, ApJ, 530, 966

Li, W.D., et al. 1999, AJ, 117, 2709

Li, W., Filippenko, A.V., Treffers, R.R., Riess, A.G., Hu, J., & Qiu, Y. 2001a, ApJ, 546, 734

Li, W., et al. 2001b, PASP, 113, 1178

Li, W., et al. 2003, PASP, 115, 453

Lira, P. 1995, Master thesis, University of Chile

Lira, P., et al. 1998, AJ, 115, 234

Macri, L.M., Stetson, P.B., Bothun, G.D., Freedman, W.L., Garnavich, P.M., Jha, S., Madore, B.F., & Richmond, M.W. 2001, ApJ, 559, 243

Misra, K., Kamble, A. P., Bhattacharya, D., Sagar, R. 2005, MNRAS, 360, 662

Nugent, P., Kim A., & Perlmutter, S. 2002, PASP, 114, 803

Nugent, P., et al. 1995, ApJ, 455, L147

Parodi, B. R., et al. 2000, ApJ, 540, 634

Patat, F., Benetti, S., Cappellaro, E., Danziger, I. J., della Valle, M., Mazzali, P. A., Turatto, M. 1996, MNRAS, 278, 111

Perlmutter, S., et al. 1997, ApJ, 483, 565

Perlmuttler, S., et al. 1999, ApJ, 517, 565

Pierce, M. J., Jacoby, G. H. 1995, AJ, 110, 2885

Phillips, M. M., et al. 1987, PASP, 99, 592

Phillips, M. M., et al. 1992, AJ, 103, 1632

Phillips, M. M. 1993, ApJ, 413, L105

Phillips, M. M., et al. 1999, AJ, 118, 1766 (P99)

Phillips, M. M., et al. 2006, astro-ph/0601684

Pignata, G., et al. 2004,MNRAS, 355, 178

Reindl, B., Tammann, G. A., Sandange, A., & Saha, A. 2005, ApJ, 624, 532 (R05)

Richmond, M. W., et al. 1995, AJ, 109, 2121

Riess, A. G., Press, W. H., Kirshner, R. P. 1996a, ApJ, 473, 588

Riess, A. G., Press, W. H., & Kirshner, R. P. 1996b, ApJ, 473, 88

Riess, A. G., et al. 1998, AJ, 116, 1009

Riess, A. G., et al. 1999, AJ, 117, 707

Riess, A.G., et al. 2004, ApJ, 607, 665

Riess, A. G., et al. 2005, ApJ, 627, 579

Saha, A., Sandage, A., Labhardt, L., Tammann, G.A., Macchetto, F.D., & Panagia, N. 1996, ApJS, 107, 693

Saha, A., Sandage, A., Labhardt, L., Tammann, G.A., Macchetto, F.D., & Panagia, N. 1997, ApJ, 486, 1

Saha, A., Sandage, A., Tammann, G.A., Labhardt, L., Macchetto, F.D., & Panagia, N. 1999, ApJ, 522, 802

Saha, A., Sandage, A., Thim, F., Labhardt, L., Tammann, G.A., Christensen, J., Panagia, N., & Macchetto, F. D. 2001a, ApJ, 551, 973

Saha, A., Sandage, A., Tammann, G.A., Dolphin, A.E., Christensen, J., Panagia, N., & Macchetto, F.D. 2001b, ApJ, 562, 314

Saha, A., Thim, F., Tammann G. A., Reindl, B., Sandange A. 2006, ApJ, in press (astro-ph/0602572)

Sakai, S., Ferranrese, L., Kennicutt, R. C., &Saha, A. 2004, ApJ, 608, 42

Sahu, D. K., Anupama, G. C., & Prabhu, T. P. 2005, MNRAS, 366, 682

Salvo, M. E., Cappellaro, E., Mazzali, P. A., Benetti, S., Danziger, I. J., Patat, F., Turatto, M. 2001, MNRAS, 321, 254

Schaefer, B.E. 1994, ApJ, 426, 493

Schaefer, B.E. 1995, ApJ, 449, L9

Schaefer, B.E. 1998, ApJ, 509, 80

Sebo, K. M., et al. 2002, ApJS, 142, 71

Spergel, D. N., et al. 2003, ApJS, 148, 175

Schlegel, D. J., Finkbeiner, D. P., & Davis, M. 1998, ApJ, 500, 525

Stritzinger, M., et al. 2002, AJ, 124, 2100

Strolger, L.-G., et al. 2002, AJ, 124, 2905

Spergel, D. N., et al. 2003, ApJS, 148, 175

Stritzinger, M., et al. 2002, AJ, 124, 2100

Strolger, L. G. et al. 2002, AJ, 124, 2905

Tripp, R. 1998, A&A, 325, 871

Tripp, R., & Branch, D. 1999, ApJ, 525, 209

Turatto, M., Piemonte, A., Benetti, S., Cappellaro, E., Mazzali, P. A., Danziger, I. J., Patat, F. 1998, AJ, 116, 2431 A

Tonry, J. L., et al. 2003, ApJ, 594, 1

Valentini, G., et al. 2003, ApJ, 595, 779

Udalski, A., et al. 1999, Acta. Astron., 49, 223

Umeda, H., et al. 1999, ApJ, 522, L43

Valentini, G., et al. 2003, ApJ, 595, 779

Vazdekis, A., Peletier, R. F., Beckman, J. E., & Vasuso E. 1997, ApJS, 111, 203

Vinko, J., et al. 2003, A&A, 115

Wang, L. F., Höflich, P., & Wheeler, J. C. 1997, ApJ, 483, L29

Wang, L. F., et al. 2003 ApJ, 590, 944

Wang, L. F. 2005, ApJ, 635, L33

Wang, L. F., et al. 2005, astro-ph/0512370

Wang, X. F., et al. 2005, ApJ, 620, L87 (W05)

Wells, L.A., et al. 1994, AJ, 108, 2233

Worthey, G. 1994, ApJS, 95, 107

Zehavi, I., Riess, A. G., Kirshner, R. P., & Dekel, A. 1998, ApJ, 503, 483

Table 1. Parameters of well-observed nearby SNe Ia.

SN	Galaxy	$v_{\rm CMB/220}$	$U_{\rm max}$	$B_{\rm max}$	$V_{\rm max}$	$I_{\rm max}$	Δm_{15}	ΔC_{12}	$E(B\text{-}V)$ Gal	$E(B\text{-}V)$ tail	$E(B\text{-}V)$ ΔC_{12}	$E(B\text{-}V)$ host	Ref.
(1)	(2)	(3)	(4)	(5)	(6)	(7)	(8)	(9)	(10)	(11)	(12)	(13)	(14)
1937C	IC 4182	330	···	8.74(09)	8.77(11)	···	0.87(10)	0.21(05)	0.014	0.04(05)	0.03(06)	0.04(04)	1,2
1972E	NGC 5253	167	7.44(20)	8.11(10)	8.17(09)	···	0.87(10)	0.24(05)	0.056	0.05(05)	0.06(06)	0.05(04)	3
1974G	NGC 4414	655	···	12.45(16)	12.34(19)	···	1.03(10)	0.47(07)	0.018	0.07(17)	0.17(08)	0.15(07)	4
1981B	NGC 4536	1179	11.72(12)	11.96(08)	11.92(07)	···	1.11(07)	0.47(05)	0.018	0.10(14)	0.13(06)	0.12(05)	5
1986G	NGC 5128	317	12.57(12)	11.95(08)	11.07(07)	···	1.73(05)	1.49(05)	0.115	0.54(06)	0.60(06)	0.57(04)	6,7
1989B	NGC 3627	549	12.15(11)	12.20(07)	11.88(06)	11.64(06)	1.35(05)	0.82(04)	0.032	0.48(16)	0.41(06)	0.42(06)	8
1990N	NGC 4639	1179	12.24(09)	12.64(07)	12.64(05)	12.89(04)	1.06(03)	0.36(02)	0.026	0.16(05)	0.05(05)	0.11(04)	9
1990O	MCG 3-44-03	9175	···	16.19(10)	16.22(08)	16.56(09)	0.96(10)	0.32(03)	0.093	0.07(06)	0.04(05)	0.05(04)	10
1990af	Anon 213562	14966	···	17.77(07)	17.75(06)	···	1.62(05)	0.62(04)	0.035	0.00(10)	−0.02(06)	0.00(04)	10
1991T†	NGC 4527	1179	11.16(09)	11.60(07)	11.44(06)	11.63(05)	0.95(05)	0.48(05)	0.022	0.15(05)	0.22(06)	0.18(04)	9
1991ag	IC 4919	4161	···	14.35(14)	14.36(16)	14.68(16)	0.88(10)	0.22(05)	0.062	0.09(07)	0.01(07)	0.05(05)	10
1991bg‡	NGC 4374	1179	···	14.58(08)	13.83(07)	13.43(06)	1.93(05)	1.51(08)	0.040	0.00(09)	0.06(08)	0.04(07)	10
1992A	NGC 1992A	1338	···	12.50(07)	12.50(07)	12.77(06)	1.47(05)	0.51(03)	0.018	0.00(03)	0.02(04)	0.02(03)	10,11
1992P	IC 3690	7939	···	16.05(07)	16.09(06)	16.38(08)	0.87(10)	0.22(03)	0.021	0.10(05)	0.03(05)	0.07(04)	10
1992ae	Anon 2128-61	22366	···	18.57(10)	18.43(08)	···	1.47(10)	0.51(05)	0.036	0.04(11)	0.02(06)	0.02(05)	10
1992ag	ESO 508-G67	8095	···	16.23(08)	16.16(07)	16.38(06)	1.10(10)	0.45(05)	0.097	0.45(20)	0.12(06)	0.15(07)	10
1992al	ESO 234-G69	4214	···	14.44(07)	14.54(06)	14.88(06)	1.11(05)	0.31(03)	0.034	0.05(05)	−0.02(05)	0.00(04)	10
1992aq	Anon 2304-37	30014	···	19.31(12)	19.29(08)	19.46(12)	1.33(10)	0.49(05)	0.012	0.03(26)	0.09(07)	0.09(07)	10
1992bc	ESO 300-G9	5876	···	15.04(07)	15.17(06)	15.51(05)	0.87(05)	0.12(03)	0.022	−0.03(05)	−0.07(05)	0.00(04)	10
1992bg	Anon 0741-62	10936	···	16.59(08)	16.67(07)	16.98(06)	1.09(10)	0.29(04)	0.185	0.05(05)	−0.03(06)	0.01(04)	10
1992bh	Anon 0459-58	13519	···	17.64(08)	17.53(06)	17.71(07)	1.07(10)	0.51(05)	0.022	0.12(08)	0.19(07)	0.18(05)	10
1992bk	ESO 156-G8	17237	···	18.01(12)	18.05(12)	18.24(11)	1.60(10)	0.62(08)	0.015	−0.01(10)	−0.01(09)	0.00(05)	10
1992bl	ESO 291-G11	12661	···	17.30(08)	17.32(07)	17.57(06)	1.49(10)	0.51(05)	0.011	0.04(06)	0.02(07)	0.03(04)	10
1992bo	ESO 352-G57	5445	···	15.74(07)	15.76(06)	15.92(05)	1.69(05)	0.70(03)	0.027	−0.01(12)	−0.07(05)	0.00(05)	10
1992bp	Anon 0336-18	23557	···	18.29(07)	18.30(06)	18.58(07)	1.32(10)	0.38(06)	0.069	0.01(21)	−0.00(07)	0.00(07)	10
1992br	Anon 0145-56	26259	···	19.31(17)	19.19(10)	···	1.66(10)	0.71(06)	0.026	0.03(23)	−0.01(08)	0.00(10)	10
1992bs	Anon 0329-37	18787	···	18.33(09)	18.25(07)	···	1.34(10)	0.50(04)	0.011	0.07(10)	0.11(06)	0.09(05)	10
1993B	Anon 1034-34	21011	···	18.37(11)	18.39(09)	18.55(11)	1.20(10)	0.46(05)	0.079	0.27(18)	0.10(07)	0.12(07)	10
1993H	ESO 445-G66	7523	···	16.73(07)	16.52(06)	16.51(06)	1.69(10)	0.82(05)	0.060	0.06(05)	0.04(07)	0.05(04)	10
1993O	Anon 1331-33	15867	···	17.56(07)	17.66(06)	17.89(06)	1.26(05)	0.41(03)	0.053	0.05(07)	0.03(05)	0.04(04)	10
1993ac	PGC 17787	14674	···	17.75(16)	17.71(12)	17.83(11)	1.43(10)	0.55(06)	0.163	−0.02(10)	0.09(07)	0.05(06)	12
1993ag	Anon 1003-35	15013	···	17.81(08)	17.73(06)	18.03(06)	1.36(10)	0.57(05)	0.112	0.12(08)	0.15(07)	0.14(05)	10
1994D	NGC 4526	1179	11.18(09)	11.75(07)	11.83(06)	12.11(05)	1.27(05)	0.34(03)	0.022	0.05(08)	−0.03(05)	0.00(04)	13,14
1994M	NGC 4493	7289	···	16.24(08)	16.22(07)	16.35(06)	1.44(10)	0.54(04)	0.023	0.13(06)	0.07(06)	0.10(04)	12
1994S	NGC 4495	4829	···	14.71(07)	14.77(06)	15.08(06)	1.02(10)	0.26(05)	0.021	0.00(10)	0.04(07)	0.00(07)	12
1994T	PGC 46640	10703	···	17.34(09)	17.16(08)	17.35(07)	1.55(10)	0.69(10)	0.029	0.07(20)	0.13(07)	0.12(07)	12
1994ae	NGC 3370	1575	12.28(12)	12.89(07)	12.94(06)	13.25(05)	0.89(05)	0.22(02)	0.031	0.03(05)	0.00(05)	0.02(04)	15
1995D	NGC 2962	2129	···	13.18(07)	13.23(06)	13.58(05)	1.00(05)	0.31(03)	0.058	0.09(05)	0.02(05)	0.06(03)	12
1995E	NGC 2441	3510	···	16.70(07)	16.01(06)	15.28(05)	1.15(05)	1.09(05)	0.027	0.73(15)	0.74(07)	0.74(06)	12
1995ac†	Anon 2245-08	14635	···	17.04(07)	17.07(06)	17.28(06)	0.91(05)	0.21(05)	0.042	0.04(07)	−0.03(06)	0.00(05)	12
1995al	NGC 3021	1851	···	13.26(07)	13.22(06)	13.50(05)	0.95(05)	0.37(03)	0.014	0.18(05)	0.12(05)	0.15(04)	12
1995ak	IC 1844	6589	···	16.00(08)	15.91(09)	16.12(09)	1.35(10)	0.51(03)	0.038	0.20(12)	0.10(05)	0.11(05)	12
1995bd†	UGC 3151	4326	···	15.16(07)	14.92(06)	15.03(06)	1.01(05)	0.54(03)	0.498	0.18(05)	0.24(05)	0.21(04)	12
1996C	MCG 8-25-47	9036	···	16.48(10)	16.49(10)	16.65(08)	0.94(10)	0.34(05)	0.013	0.08(06)	0.09(07)	0.08(05)	12
1996X	NGC 5061	2120	···	12.96(07)	12.97(06)	13.23(05)	1.33(05)	0.44(02)	0.069	0.06(05)	0.04(04)	0.05(03)	12,16
1996Z	NGC 2935	2285	···	14.32(07)	14.00(06)	···	1.06(10)	0.68(05)	0.064	···	0.37(06)	0.37(06)	12
1996ab	Anon 1521+28	37370	···	19.54(09)	19.43(08)	···	1.16(05)	0.38(10)	0.032	0.03(08)	0.05(10)	0.04(07)	12
1996ai	NGC 5005	1298	···	16.90(08)	15.17(09)	13.93(10)	1.02(10)	1.92(05)	0.014	2.03(14)	1.63(06)	1.69(06)	12
1996bk	NGC 5308	2462	···	14.70(09)	14.40(11)	14.26(08)	1.69(10)	1.00(07)	0.018	0.31(13)	0.23(08)	0.26(07)	12
1996bl	Anon 0036+11	10447	···	16.68(07)	16.68(07)	16.87(07)	1.11(10)	0.36(04)	0.092	0.13(07)	0.03(06)	0.07(04)	12
1996bo	NGC 673	4898	···	15.82(07)	15.53(06)	15.52(06)	1.30(05)	0.72(03)	0.077	0.30(10)	0.34(05)	0.33(04)	11,12
1996bv	UGC 3432	5016	···	15.34(13)	15.14(10)	15.35(09)	0.95(10)	0.44(06)	0.105	0.21(10)	0.18(07)	0.19(05)	12
1997E	NGC 2258	3998	14.74(09)	15.05(08)	15.02(07)	15.17(06)	1.44(05)	0.56(05)	0.124	0.07(05)	0.10(07)	0.09(04)	17
1997Y	NGC 4675	4968	14.82(10)	15.26(08)	15.24(08)	15.38(06)	1.26(10)	0.47(05)	0.017	0.08(05)	0.10(06)	0.09(04)	17
1997bp	NGC 4680	2647	13.84(09)	13.89(07)	13.72(06)	14.03(05)	1.19(06)	0.58(05)	0.044	0.14(05)	0.22(07)	0.17(04)	11,17
1997bq	NGC 3147	2879	14.10(10)	14.44(11)	14.24(08)	14.39(10)	1.11(10)	0.54(05)	0.032	0.17(05)	0.24(07)	0.19(04)	17
1997br†	ESO 579-G40	2193	13.00(15)	13.61(10)	13.40(08)	13.42(20)	1.15(10)	0.75(03)	0.113	0.31(05)	0.41(05)	0.36(04)	17,18
1997cn‡	NGC 5490	5246	16.89(20)	16.89(15)	16.35(10)	16.21(10)	1.88(10)	1.28(06)	0.027	0.06(13)	0.00(07)	0.01(06)	17,19
1997dg	Anonymous	9845	16.31(10)	16.83(07)	16.84(07)	16.92(06)	1.19(10)	0.44(05)	0.078	0.29(20)	0.09(06)	0.11(07)	17
1997do	UGC 3845	3135	14.00(15)	14.32(11)	14.28(07)	14.52(07)	0.99(10)	0.40(06)	0.063	0.16(08)	0.13(08)	0.15(06)	17
1998V	NGC 6627	5161	14.53(10)	15.06(08)	15.05(07)	15.27(06)	1.08(10)	0.35(04)	0.196	0.08(05)	0.03(06)	0.06(04)	17
1998ab†	NGC 4704	8354	15.59(12)	16.05(09)	16.06(08)	16.29(08)	1.12(10)	0.39(03)	0.017	0.18(07)	0.05(05)	0.09(04)	17
1998aq	NGC 3982	1514	11.63(09)	12.30(07)	12.41(06)	12.69(05)	1.05(03)	0.28(03)	0.014	−0.03(05)	0.07(04)	0.03(04)	17
1998bp‡	NGC 6495	3048	15.21(10)	15.32(10)	15.02(08)	14.91(08)	1.83(05)	1.06(05)	0.076	0.06(05)	−0.03(07)	0.02(04)	17
1998bu	NGC 3368	810	11.77(09)	12.11(07)	11.80(06)	11.59(05)	1.02(03)	0.64(03)	0.025	0.37(05)	0.34(05)	0.36(04)	17
1998de‡	NGC 252	4713	17.90(20)	17.31(07)	16.63(06)	16.48(08)	1.95(09)	1.58(06)	0.058	0.00(10)	0.03(07)	0.02(06)	17,20
1998dh	NGC 7541	2766	13.53(20)	13.81(08)	13.74(07)	13.92(07)	1.28(10)	0.53(06)	0.068	0.15(05)	0.15(07)	0.15(04)	17
1998dx	UGC 11149	14895	17.03(16)	17.53(12)	17.64(10)	17.75(09)	1.47(10)	0.43(05)	0.041	−0.04(08)	−0.05(07)	0.00(06)	17
1998eg	UGC 12133	7067	15.63(16)	16.07(07)	16.07(06)	16.24(06)	1.13(05)	0.44(04)	0.123	0.08(10)	0.10(06)	0.09(06)	17
1998es†	NGC 632	2872	13.28(09)	13.81(07)	13.73(06)	14.00(05)	0.88(05)	0.33(04)	0.032	0.17(06)	0.13(06)	0.15(05)	17
1999aa†	NGC 2595	4572	14.15(09)	14.71(07)	14.73(06)	15.13(05)	0.82(05)	0.19(03)	0.040	0.04(05)	0.05(05)	0.05(04)	17
1999ac†	NGC 6063	2950	13.77(09)	14.07(09)	14.05(07)	14.22(06)	1.35(05)	0.58(05)	0.046	0.07(07)	0.17(07)	0.12(06)	17,21

Table 1—Continued

SN	Galaxy	$v_{\rm CMB/220}$	$U_{\rm max}$	$B_{\rm max}$	$V_{\rm max}$	$I_{\rm max}$	Δm_{15}	ΔC_{12}	$E(B\text{-}V)$ Gal	$E(B\text{-}V)$ tail	$E(B\text{-}V)$ ΔC_{12}	$E(B\text{-}V)$ host	Ref.
(1)	(2)	(3)	(4)	(5)	(6)	(7)	(8)	(9)	(10)	(11)	(12)	(13)	(14)
1999aw†	Anon 1101-06	12363	···	16.72(07)	16.70(06)	17.17(05)	0.81(03)	0.16(03)	0.032	0.00(10)	0.04(05)	0.04(05)	17,22
1999by‡	NGC 2841	896	13.73(09)	13.59(07)	13.10(06)	12.88(05)	1.90(05)	1.29(06)	0.016	0.00(04)	−0.06(07)	0.00(03)	17,23
1999cc	NGC 6038	9461	16.56(10)	16.77(10)	16.74(09)	16.88(09)	1.45(10)	0.54(04)	0.023	0.02(06)	0.07(06)	0.05(04)	17,24
1999cl	NGC 4501	1179	15.57(10)	14.86(12)	13.73(08)	13.00(07)	1.29(10)	1.55(06)	0.038	1.24(06)	1.16(07)	1.20(05)	17,24
1999cp	NGC 5468	3109	···	13.94(09)	13.96(08)	14.19(07)	1.05(10)	0.34(06)	0.024	···	0.03(07)	0.03(07)	17
1999da‡	NGC 6411	3644	···	16.61(09)	16.03(09)	15.73(08)	1.94(10)	1.46(06)	0.058	0.05(20)	−0.04(08)	0.00(07)	24
1999dk	UGC 1087	4184	14.47(13)	14.81(09)	14.76(07)	15.10(06)	0.99(10)	0.41(05)	0.054	0.15(21)	0.11(07)	0.11(06)	11,24
1999dq†	NGC 976	4066	13.86(09)	14.41(07)	14.33(06)	14.57(05)	0.95(05)	0.34(05)	0.110	0.15(07)	0.07(07)	0.11(05)	11,17
1999ee	IC 5179	3153	14.63(09)	14.84(07)	14.54(06)	14.62(05)	0.94(05)	0.54(03)	0.020	0.38(06)	0.29(05)	0.33(04)	24,25
1999ej	NGC 495	3839	14.98(20)	15.30(09)	15.37(07)	15.53(06)	1.39(10)	0.47(05)	0.072	−0.02(17)	0.04(07)	0.02(06)	17
1999ek	UGC 3329	5271	···	15.53(07)	15.42(05)	15.53(05)	1.13(03)	0.49(03)	0.553	0.20(08)	0.16(05)	0.17(04)	17,24
1999gd	NGC 2623	5761	16.82(16)	16.88(08)	16.47(07)	16.19(08)	1.13(10)	0.82(06)	0.041	0.45(16)	0.48(07)	0.48(06)	17
1999gh	NGC 2986	2314	13.88(20)	14.21(16)	14.13(12)	14.13(10)	1.69(10)	0.86(06)	0.059	0.07(05)	0.08(07)	0.07(04)	17
1999gp†	UGC 1993	7811	15.47(10)	16.01(08)	15.95(07)	16.23(06)	0.92(10)	0.33(05)	0.056	0.11(10)	0.09(07)	0.10(06)	17
2000E	NGC 6951	1824	12.50(10)	12.72(07)	12.63(06)	12.77(07)	0.96(05)	0.35(04)	0.366	0.25(10)	0.09(06)	0.13(05)	26
2000bh	ESO 573-G014	7238	···	15.86(08)	15.89(07)	16.24(05)	1.16(10)	0.42(05)	0.048	0.07(06)	0.08(07)	0.07(05)	17
2000ca	ESO 383-G032	7080	14.96(10)	15.53(07)	15.62(06)	15.93(05)	0.96(05)	0.22(03)	0.067	0.02(05)	−0.03(05)	0.00(04)	24
2000ce	UGC 4195	4940	16.76(20)	16.99(16)	16.41(16)	16.04(12)	1.00(10)	0.85(06)	0.057	0.73(15)	0.56(07)	0.59(06)	17,24
2000cf	MCG 11-19-25	10805	16.59(12)	17.00(09)	17.02(08)	17.21(07)	1.27(10)	0.44(04)	0.032	0.11(05)	0.06(05)	0.09(04)	17,24
2000cn	UGC 11064	6971	16.47(10)	16.56(08)	16.40(07)	16.57(05)	1.59(10)	0.73(04)	0.057	0.12(06)	0.12(06)	0.12(05)	17
2000cx†	NGC 524	2454	12.74(09)	13.06(07)	12.98(06)	13.49(06)	0.93(05)	0.32(05)	0.083	−0.21(05)	0.06(06)	0.00(04)	17,27
2000dk	NGC 382	4929	15.04(09)	15.33(07)	15.34(06)	15.59(05)	1.63(05)	0.67(07)	0.070	−0.03(06)	0.00(08)	0.00(05)	17
2000fa	UGC 3770	6526	15.39(20)	15.70(10)	15.72(10)	15.94(08)	0.98(10)	0.35(05)	0.069	0.12(08)	0.08(07)	0.10(06)	17
2001V†	NGC3987	4804	···	14.55(12)	14.53(09)	14.82(08)	0.95(05)	0.28(04)	0.020	0.02(10)	0.01(06)	0.01(06)	29
2001ay*	IC 4423	9269	···	16.61(07)	16.62(06)	16.67(06)	0.69(05)	0.38(04)	0.019	···	···	0.04(05)	28
2001ba	MCG-05-28-001	9245	···	16.17(08)	16.27(09)	16.58(07)	0.98(05)	0.27(05)	0.064	−0.01(10)	−0.01(07)	0.00(05)	24
2001bt	IC 4830	4332	···	15.25(07)	15.10(05)	15.18(05)	1.28(05)	0.63(03)	0.065	0.26(06)	0.25(05)	0.25(04)	24
2001cn	IC 4758	4628	14.99(18)	15.20(07)	15.11(05)	15.21(05)	1.15(05)	0.51(03)	0.059	0.21(07)	0.16(05)	0.17(04)	24
2001cz	NGC 4679	4900	···	15.03(07)	14.97(05)	15.14(05)	1.07(03)	0.36(03)	0.092	0.17(06)	0.04(05)	0.09(04)	24
2001el	NGC 1448	1030	12.59(09)	12.75(07)	12.68(06)	12.79(06)	1.13(03)	0.58(02)	0.014	0.29(05)	0.24(05)	0.27(04)	24
2002bo	NGC 3190	1547	···	13.93(10)	13.50(10)	13.47(10)	1.13(05)	0.74(05)	0.025	0.43(06)	0.40(07)	0.42(05)	30
2002cx*	CGCG 044-035	7488	···	17.56(10)	17.46(16)	17.29(10)	1.28(10)	0.60(05)	0.032	0.14(21)	0.20(07)	0.19(07)	27
2002el	NGC 6986	7079	···	16.11(07)	16.16(06)	16.37(07)	1.32(05)	0.49(03)	0.085	0.28(18)	0.09(05)	0.10(05)	31
2002er	UGC 10743	2652	13.86(09)	14.21(07)	14.07(06)	14.18(07)	1.33(04)	0.59(05)	0.157	0.21(06)	0.19(06)	0.20(06)	32
2002hu	MCG+06-06-012	11000	16.42(09)	16.63(07)	16.68(06)	16.93(07)	1.03(05)	0.31(04)	0.044	0.09(05)	0.01(05)	0.05(04)	33
2003du	UGC 9391	2008	13.00(09)	13.49(07)	13.61(06)	13.83(07)	1.00(04)	0.22(05)	0.010	0.05(05)	−0.07(06)	0.00(04)	34
2004S	MCG-05-16-021	2516	···	14.01(08)	14.02(09)	14.32(10)	1.11(05)	0.40(05)	0.101	0.08(05)	0.07(06)	0.08(04)	35

References. — [1]Schaefer(1994), [2]Pierce & Jacoby (1995), [3]Ardeberg & Groot (1973), [4]Schaefer(1998), [5]Schaefer(1995), [6]Phillips et al.(1987), [7]Cristiani et al.(1992), [8]Wells et al. (1994), [9]Lira et al. (1998), [10]Hamuy et al. (1996a), [11]Altavilla et al.(2004), [12]Riess et al. (1999), [13]Richmond et al. (1995), [14]Patat et al. (1996), [15]Riess et al. (2005), [16]Salvo et al. (2001), [17]Jha et al.(1999; 2006a), [18]Li et al. (1999), [19]Turrato et al. (1998), [20]Modjaz et al. (2001), [21]Phillips et al. (2006), [22]Strolger et al. (2002), [23]Garnavich et al. (2004), [24]Krisciunas et al. (2001, 2003, 2004a,b, 2005), [25]Stritzinger et al. (2002), [26]Valenini et al. (2003), [27]Li et al.(2001b, 2003), [28]Howell & Nugent (2003), [29]Vinko et al. (2003), [30]Benetti et al. (2004), [31]from Weidong Li, [32]Pignata et al.(2004), [33]Sahu et al. (2006), [34] Anupama et al. (2005), [35]Misra et al. (2005).

†1991T/1999aa-like SNe.

‡1991bg-like SNe.

*SN 2001ay is the SN Ia with the broadest light curve (Howell & Nugent 2003); SN 2002cx displayed the most unique spectral and photometric features (Li et al 2003).

Table 2. Parameters relevant for SN host galaxies

SN (1)	Galaxy (2)	$z_{CMB/220}$ (3)	Type (4)	T (5)	r_{SN}/r_{25} (6)	μ_U (7)	μ_B (8)	μ_V (9)	μ_I (10)
1937C	IC 4182*	0.0011	Sm	9	0.28(03)	···	···	···	···
1972E	NGC 5253*	0.0006	Im	8	···	···	···	···	···
1974G	NGC 4414*	0.0022	Sc	5	0.55(03)	···	···	···	···
1981B	NGC 4536*	0.0039	Sbc	4	0.70(05)	···	···	···	···
1986G	NGC 5128	0.0011	S0	−2	0.23(02)	28.36(24)	28.20(19)	28.15(17)	···
1989B	NGC 3627*	0.0018	Sb	3	0.21(02)	···	···	···	···
1990N	NGC 4639*	0.0499	Sbc	4	0.84(06)	···	···	···	···
1990O	MCG+3-44-03	0.0306	Sa	1	0.82(05)	···	35.43(20)	35.43(18)	35.51(16)
1990af	Anon 213562	0.0039	Sa	1	0.00(05)	···	36.50(19)	36.57(17)	9.99(99
1991T	NGC 4527*	0.0039	Sbc	4	0.61(02)	···	···	···	···
1991ag	IC 4919	0.0039	Sdm	8	0.80(06)	···	33.78(25)	33.72(23)	33.73(21
1991bg	IC 4374	0.0139	E1	−4	0.30(02)	30.29(23)	30.35(19)	30.31(17)	30.40(14)
1992A	NGC 1380	0.0045	S0	−2	0.44(03)	···	31.41(17)	31.46(16)	31.54(14)
1992P	IC 3690	0.0265	Sb	3	0.89(13)	···	35.46(19)	35.43(17)	35.43(15)
1992ae	Anon 2128-61	0.0746	E/S0	−3	0.15(05)	···	37.48(23)	37.39(19)	9.99(99
1992ag	ESO 508-G67	0.0270	Sbc	4	···	···	35.08(27)	35.10(22)	35.18(16)
1992al	ESO 234-G69	0.0141	Sc	5	0.42(03)	···	33.77(19)	33.81(17)	33.85(14)
1992aq	Anon 2304-37	0.1001	Sa	1	0.38(10)	···	38.17(29)	38.22(22)	38.23(19)
1992bc	ESO 300-G9	0.0196	Sab	4	0.80(23)	···	34.74(19)	34.71(17)	34.67(14)
1992bg	Anon 0741-62	0.0364	Sa	1	0.18(10)	···	35.94(19)	35.96(17)	35.97(14)
1992bh	Anon 0459-58	0.0451	Sbc	4	0.11(02)	···	36.33(22)	36.36(18)	36.45(15)
1992bk	ESO 156-G8	0.0575	E/S0	−2	0.87(08)	···	36.74(24)	36.87(21)	36.90(17)
1992bl	ESO 291-G11	0.0422	S0/a	1	1.52(07)	···	36.20(19)	36.28(17)	36.33(14)
1992bo	ESO 352-G57	0.0181	S0	−2	1.74(19)	···	34.31(22)	34.47(18)	34.50(15)
1992bp	Anon 0336-18	0.0785	S0	−2	0.26(04)	···	37.48(27)	37.47(21)	37.48(16)
1992br	Anon 0145-56	0.0875	E/S0	−3	1.23(07)	···	37.86(39)	37.88(28)	···
1992bs	Anon 0329-37	0.0626	Sb	3	0.94(06)	···	37.17(22)	37.17(18)	···
1993B	Anon 1034-34	0.0700	Sb	3	0.29(03)	···	37.24(28)	37.34(22)	37.35(18)
1993H	ESO 445-G66	0.0251	Sab	2	0.35(05)	···	35.00(19)	35.01(17)	34.96(14)
1993O	Anon 1331-33	0.0529	S0	−2	1.40(40)	···	36.64(19)	36.75(17)	36.75(14)
1993ac	PGC 17787	0.0489	E	−3	0.68(10)	···	36.55(28)	36.59(22)	36.55(18)
1993ag	Anon 1003-35	0.0500	S0	−2	0.70(18)	···	36.44(22)	36.51(18)	36.71(15)
1994D	NGC 4526	0.0243	S0	−2	0.19(01)	30.99(23)	31.02(19)	31.06(17)	31.05(14)
1994M	NGC 4493	0.0161	E	−4	0.68(10)	···	34.99(19)	35.07(17)	35.07(14)
1994S	NGC 4495	0.0357	Sab	2	0.74(09)	···	34.14(27)	34.11(21	34.10(16)
1994T	PGC 46640	0.0052	Sa	1	···	···	35.77(28)	35.78(22)	35.92(16)
1994ae	NGC 3370*	0.0039	Sc	5	0.51(04)	···	···	···	···
1995D	NGC 2962	0.0144	S0	−1	1.18(06)	···	32.43(17)	32.45(16)	32.54(14)
1995E	NGC 2441	0.0117	Sb	3	0.41(03)	···	33.49(24)	33.52(20)	33.34(15)
1995ac	Anon 2245-08	0.0071	Sa	1	···	···	36.56(22)	36.48(18)	36.35(15)
1995ak	IC 1844	0.0488	Sbc	4	0.37(03)	···	34.79(22)	34.80(19)	34.87(16)
1995al	NGC 3021	0.0062	Sbc	4	0.44(05)	···	32.26(19)	32.27(17)	32.38(14)
1995bd	UGC 3151	0.0220	Sbc	4	0.79(09)	···	33.75(19)	33.68(17)	33.73(14)
1996C	MCG+8-25-47	0.0301	Sa	1	0.42(03)	···	35.64(23)	35.65(20)	35.58(16)

Table 2—Continued

SN (1)	Galaxy (2)	$z_{CMB/220}$ (3)	Type (4)	T (5)	r_{SN}/r_{25} (6)	μ_U (7)	μ_B (8)	μ_V (9)	μ_I (10)
1996X	NGC 5061	0.0071	E0	−5	0.57(03)	···	31.97(17)	32.01(16)	32.06(14)
1996Z	NGC 2935	0.0076	Sb	3	0.61(03)	···	32.42(24)	32.42(20)	···
1996ai	NGC 5005	0.1246	Sbc	4	0.16(01)	···	30.76(25)	30.67(21)	30.99(17)
1996ab	Anon 1521+28	0.0043	Sc	5	···	···	38.68(28)	38.56(22)	···
1996bk	NGC 5308	0.0082	S0	−2	···	···	32.33(28)	32.45(23)	32.49(17)
1996bl	Anon 0036+11	0.0348	Sc	5	···	···	35.82(19)	35.82(17)	35.78(15)
1996bo	NGC 673	0.0163	Sc	5	0.13(01)	···	33.90(19)	33.93(17)	34.02(14)
1996bv	UGC 3432	0.0167	Scd	6	0.07(01)	···	34.15(24)	34.06(20)	34.16(16)
1997E	NGC 2258	0.0133	S0	−2	0.95(27)	33.81(23)	33.77(19)	33.85(17)	33.87(14)
1997Y	NGC 4675	0.0166	Sb	3	0.14(02)	34.13(24)	34.15(19)	34.20(18)	34.17(14)
1997bp	NGC 4680	0.0088	Sb	3	0.57(08)	32.72(23)	32.46(19)	32.46(17)	32.70(14)
1997bq	NGC 3147	0.0096	Sbc	4	0.62(03)	33.05(24)	33.06(21)	33.02(18)	33.10(16)
1997br	ESO 576-G40*	0.0073	Sd	7	0.90(06)	31.11(26)	31.59(20)	31.73(18)	31.89(24)
1997cn	NGC 5490	0.0175	E	−5	0.22(02)	34.19(35)	34.33(28)	34.21(21)	34.21(17)
1997dg	Anonymous	0.0328	Sa	1	···	35.67(34)	35.75(27)	35.83(22)	35.74(16)
1997do	UGC 3845	0.0104	Sbc	4	0.12(01)	33.39(33)	33.27(26)	33.29(20)	33.37(16)
1998V	NGC 6627	0.0172	Sb	3	0.86(10)	34.21(24)	34.23(19)	34.21(17)	34.19(14)
1998ab	NGC 4704	0.0279	Sbc	4	0.51(04)	35.11(24)	35.10(20)	35.14(18)	35.16(15)
1998aq	NGC 3982*	0.0050	Sb	3	0.32(02)	···	···	···	···
1998bp	NGC 6495	0.0102	E	−5	0.21(04)	33.08(24)	33.17(20)	33.19(18)	33.13(15)
1998bu	NGC 3368*	0.0027	Sab	2	0.24(01)	···	···	···	···
1998de	NGC 252	0.0157	S0	−1	1.60(19)	34.39(35)	34.15(24)	34.05(20)	34.18(16)
1998dh	NGC 7541	0.0092	Sbc	4	0.52(02)	32.58(29)	32.50(19)	32.56(17)	32.64(15)
1998dx	UGC 11149	0.0496	Sb	3	0.95(05)	36.60(33)	36.63(26)	36.74(21)	36.60(17)
1998eg	UGC 12133	0.0236	Sc	6	0.70(07)	35.02(33)	35.02(24)	35.08(20)	35.06(15)
1998es	NGC 632	0.0096	S0	−2	0.23(03)	32.86(26)	32.89(22)	32.84(18)	32.92(15)
1999aa	NGC 2595	0.0152	Sc	5	0.38(03)	34.27(23)	34.20(19)	34.13(17)	34.21(14)
1999ac	NGC 6063	0.0098	Scd	6	0.85(10)	32.74(30)	32.71(25)	32.83(20)	32.90(15)
1999aw	Anon 1101-06	0.0412	?	?	···	···	36.29(22)	36.15(18)	36.28(15)
1999by	NGC 2841*	0.0030	Sb	3	0.66(02)	···	···	···	···
1999cc	NGC 6038	0.0315	Sc	5	0.50(07)	35.75(24)	35.58(20)	35.64(18)	35.61(16)
1999cl	NGC 4501*	0.0039	Sb	3	0.30(01)	30.12(27)	30.12(24)	30.18(19)	30.51(15)
1999cp	NGC 5468	0.0104	Scd	6	0.72(03)	···	33.17(28)	33.16(22)	33.12(16)
1999da	NGC 6411	0.0121	E	−5	1.03(030	···	33.71(28)	33.64(22)	33.55(17)
1999dk	UGC 1087	0.0139	Sc	5	0.64(08)	33.91(32)	33.79(25)	33.79(20)	33.95(15)
1999dq	NGC 976	0.0136	Sc	5	0.19(01)	33.48(27)	33.53(22)	33.46(18)	33.49(15)
1999ee	IC 5179	0.0105	Sbc	4	0.31(02)	33.34(23)	33.26(19)	33.19(17)	33.30(14)
1999ej	NGC 495	0.0128	S0/a	0	0.80(10)	34.41(35)	34.29(25)	34.39(20)	34.34(15)
1999ek	UGC 3329	0.0176	Sbc	4	0.70(12)	···	34.27(19)	34.28(16)	34.29(14)
1999gd	NGC 2623	0.0192	Sab	2	0.28(04)	34.54(33)	34.55(25)	34.59(20)	34.56(16)
1999gh	NGC 2986	0.0077	E	−5	0.57(04)	32.19(29)	32.38(24)	32.55(20)	32.54(16)
1999gp	UGC 1993	0.0260	Sb	3	0.28(03)	35.14(31)	35.16(25)	35.11(20)	35.16(15)
2000E	NGC 6951	0.0061	Sbc	4	0.25(01)	32.06(27)	31.79(22)	31.73(18)	31.68(15)
2000bh	ESO 573-G014	0.0241	Sc	5	0.50(22)	···	34.88(22)	34.94(18)	35.09(15)
2000ca	ESO 383-G032	0.0236	Sbc	4	0.25(04)	35.09(24)	35.03(19)	35.02(17)	34.99(14)

Table 2—Continued

SN (1)	Galaxy (2)	$z_{CMB/220}$ (3)	Type (4)	T (5)	r_{SN}/r_{25} (6)	μ_U (7)	μ_B (8)	μ_V (9)	μ_I (10)
2000ce	UGC 4195	0.0165	Sb	3	0.51(07)	34.21(35)	34.45(28)	34.40(25)	34.36(18)
2000cf	MCG+11-19-25	0.0360	Sbc	4	0.55(25)	35.98(24)	35.95(20)	36.03(18)	36.03(15)
2000cn	UGC 11064	0.0232	Scd	6	0.17(03)	35.04(27)	34.91(22)	34.96(18)	35.10(15)
2000cx	NGC 524	0.0082	S0	−1	···	32.60(23)	32.37(19)	32.24(17)	32.45(14)
2000dk	NGC 382	0.0164	E	−5	0.51(19)	33.98(26)	33.96(22)	34.09(18)	34.20(15)
2000fa	UGC 3770	0.0217	Im	10	0.40(09)	35.00(35)	34.81(25)	34.85(21)	34.85(16)
2001V	NGC 3987	0.0160	Sb	3	0.96(09)	···	33.92(26)	33.83(21)	33.82(16)
2001ay	IC 4423	0.0309	Sbc	4	0.69(10)	···	35.75(22)	35.75(18)	35.56(15)
2001ba	MCG-05-28-001	0.0308	Sbc	4	0.85(08)	···	35.58(22)	35.60(19)	35.59(15)
2001bt	IC 4830	0.0144	Sbc	4	0.57(05)	···	33.61(19)	33.69(16)	33.78(14)
2001cn	IC 4758	0.0154	Sc	5	0.73(08)	34.06(28)	33.91(19)	33.95(16)	33.95(14)
2001cz	NGC 4679	0.0163	Sc	4	0.44(04)	···	34.14(19)	34.09(16)	34.04(14)
2001el	NGC 1448	0.0034	Scd	6	···	31.30(23)	31.18(19)	31.33(17)	31.44(14)
2002bo	NGC 3190	0.0052	Sa	1	0.17(01)	···	31.84(23)	31.79(20)	31.93(17)
2002cx	CGCG 044-035	0.0250	?	?	···	···	36.06(28)	36.15(26)	35.94(18)
2002el	NGC 6986	0.0236	E/S0	−3	0.86(07)	···	34.95(22)	35.08(18)	35.14(15)
2002er	UGC 10743	0.0088	Sa	1	0.38(04)	32.67(30)	32.72(24)	32.76(20)	32.83(16)
2002hu	MCG+06-06-012	0.0367	Sc	5	1.17(10)	36.22(23)	35.89(19)	35.91(17)	35.89(15)
2003du	UGC 9391	0.0067	Sdm	8	0.34(03)	33.13(23)	32.99(19)	33.01(17)	32.89(15)
2004S	MCG-05-16-21	0.0084	Sc	5	1.13(05)	···	33.05(19)	33.09(18)	33.19(16)

*Host galaxies for which a Cepheid distance is available.

*The dust in ESO 576-G40 and NGC 4501 may be very different from that of the other distant galaxies (see the discussions in the text), so the distance moduli presented here for them may not represent their true distances.

Table 3. The coefficients of the relations between peak luminosity, color parameter ΔC_{12} and the host-galaxy reddening.

Bandpass	N[a]	b	R	M^0	σ_M
U	29	2.65(10)	4.37(25)	−19.87(05)	0.162
B	73	1.94(06)	3.33(11)	−19.34(02)	0.120
V	73	1.44(06)	2.30(11)	−19.27(02)	0.117
I	69	1.00(05)	1.18(11)	−18.96(02)	0.112

[a]N is the number of Hubble flow SN Ia sample used to determine the relation.

Table 4. The best-fitting results of the $m - z$ relation for different SN Ia sample.

Sample	N^a_{BV}	α_U	σ_U	α_B	σ_B	α_V	σ_V	α_I	σ_I
All	73	−4.18(03)	0.162	−3.64(01)	0.120	−3.56(01)	0.117	−3.25(01)	0.112
normal	58	−4.14(03)	0.113	−3.63(01)	0.104	−3.54(01)	0.099	−3.23(02)	0.091
normal, v < 7,000	26	−4.17(05)	0.113	−3.65(03)	0.118	−3.56(02)	0.108	−3.24(02)	0.102
normal, v > 7,000	32	−4.06(06)	0.104	−3.63(02)	0.093	−3.53(03)	0.091	−3.21(02)	0.081
normal, E$(B-V)_{host}$ ⩽0.15	47	−4.14(04)	0.126	−3.63(02)	0.090	−3.53(02)	0.087	−3.22(02)	0.087
normal, E$(B-V)_{host}$ ⩽0.06	24	−4.18(07)	0.177	−3.64(02)	0.078	−3.55(02)	0.074	−3.25(02)	0.071
91T/99aa-like	10	−4.28(08)	0.206	−3.70(06)	0.175	−3.69(04)	0.138	−3.35(05)	0.161
91bg-like	4	−4.14(15)	0.228	−3.55(08)	0.083	−3.56(07)	0.093	−3.26(07)	0.082

[a]N_{BV} represents the number of SN Ia sample available in the B and V bands.

Table 5. The absolute magnitudes of SNe Ia with Cepheid distances.

SN (1)	$Galaxy$ (2)	μ_{KP} (3)	μ_{KP}(Z) (4)	m_V (5)	ΔC_{12} (6)	E$(B-V)_{host}$ (7)	m^0_V (8)	M^0_U (9)	M^0_B (10)	M^0_V (11)	M^0_I (12)
1937C	IC 4182	28.28(06)	28.26(06)	8.77	0.21	0.04	8.89(13)	···	−19.38(18)	−19.38(16)	···
1972E	NGC 5253	27.56(14)	27.48(14)	8.17	0.24	0.05	8.24(12)	−19.94(30)	−19.30(22)	−19.25(19)	···
1974G	NGC 4414	31.10(05)	31.27(06)	12.34	0.47	0.15	11.99(22)	···	−19.34(29)	−19.29(26)	···
1981B	NGC 4536	30.80(04)	30.88(04)	11.92	0.47	0.12	11.59(08)	−19.79(28)	−19.40(21)	−19.29(16)	···
1989B	NGC 3627	29.86(08)	30.04(09)	11.88	0.76	0.37	10.93(10)	−19.96(29)	−19.41(23)	−19.26(18)	−18.98(13)
1990N	NGC 4639	31.61(08)	31.73(08)	12.64	0.36	0.11	12.48(08)	−19.81(21)	−19.34(17)	−19.25(14)	−18.91(11)
1991T	NGC 4527	30.48(09)	30.58(09)	11.44	0.48	0.18	11.05(09)	−20.18(21)	−19.56(18)	−19.54(15)	−19.15(12)
1994ae	NGC 3370	32.22(06)	32.29(06)	12.94	0.22	0.05	13.04(08)	−19.80(21)	−19.25(16)	−19.23(13)	−18.95(09)
1998aq	NGC 3982	31.60(09)	31.66(09)	12.41	0.28	0.03	12.43(07)	−19.98(20)	−19.35(17)	−19.23(13)	−18.95(11)
1998bu	NGC 3368	29.97(06)	30.14(07)	11.80	0.64	0.36	11.03(09)	−19.86(20)	−19.17(16)	−19.12(13)	−18.94(11)
1999by	NGC 2841	30.74(23)	30.84(23)	13.10	1.29	0.00	11.66(11)	−19.71(30)	−19.15(27)	−19.15(25)	−18.95(25)
mean								−19.89(08)	−19.33(06)	−19.27(05)	−18.97(04)
mean	(excl.	SNe 1991T,	99by)					−19.87(09)	−19.32(06)	−19.24(05)	−18.95(05)
mean	(excl.	SNe 1989B,	98bu)					−19.86(10)	−19.34(07)	−19.27(07)	−18.94(06)

Table 6. The Value of the Hubble constant H_0 (in km s^{-1} Mpc^{-1})from SNe Ia.

Sample(N_h+N_c)[a]	H_0(U)	H_0(B)	H_0(V)	H_0(I)	H_0(U,B,V,I)
All(73+11)	72.1±2.9	72.8±2.1	72.1±1.8	71.8±1.4	72.1±0.9
normal(58+9)	71.4±3.5	72.8±2.1	72.4±2.1	71.8±1.8	72.2±1.1
normal, E$(B-V)_{host}$≤0.15(47+7)	71.8±3.6	72.1±2.5	71.1±2.3	71.8±2.1	71.7±1.2
91T/99aa-like(10+1)	66.1±6.9	67.3±5.9	67.6±4.9	69.2±4.2	67.9±2.6
91bg-like(4+1)	76.9±12.0	75.9±9.9	76.2±9.8	72.8±8.7	75.1±5.0

[a]N_h is the number of the Hubble flow SN sample , while N_c is the number of the nearby calibrators.

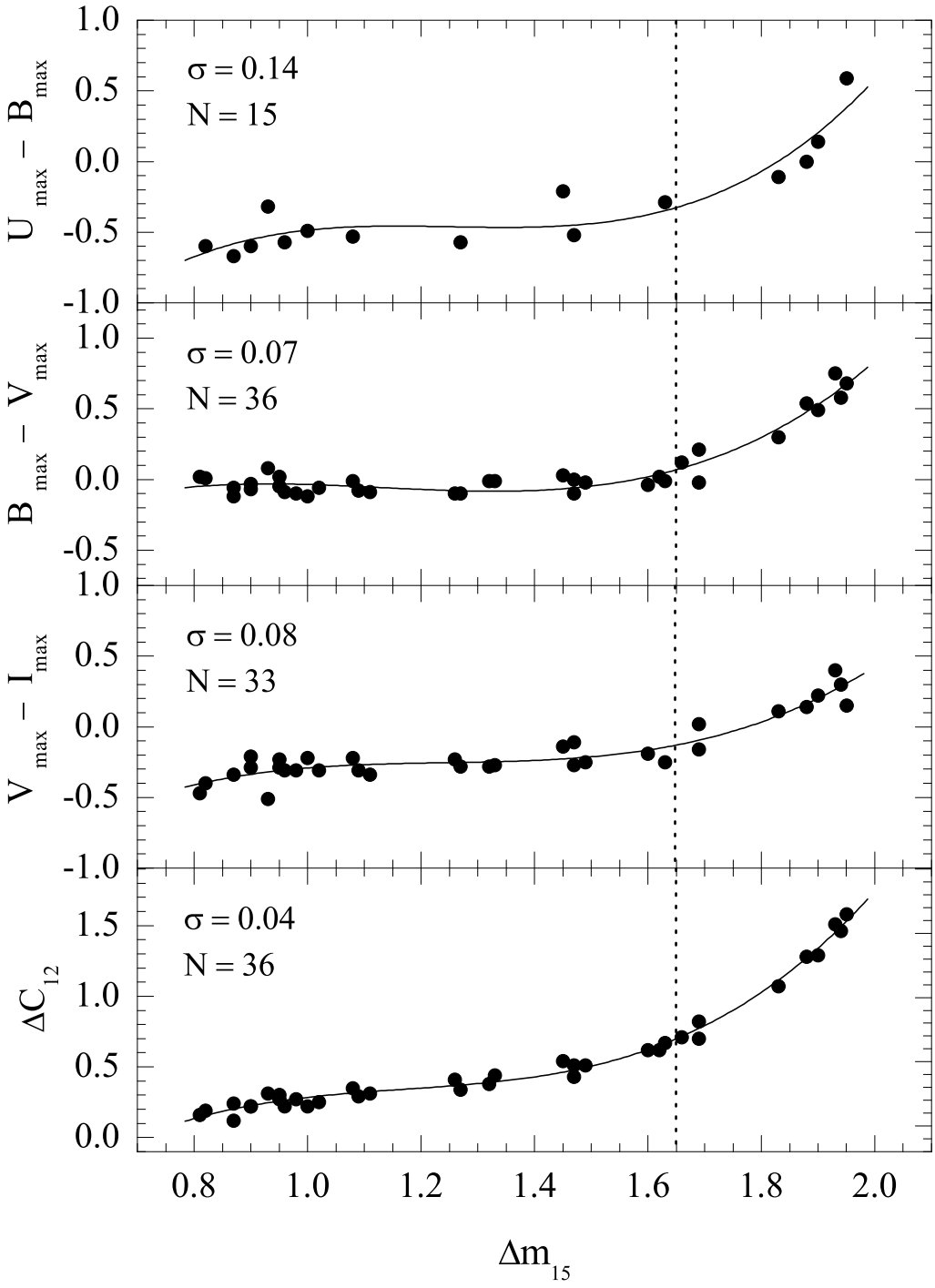

Fig. 1.— Dependence of the color parameters $U_{\max} - B_{\max}$, $B_{\max} - V_{\max}$, $V_{\max} - I_{\max}$,, and ΔC_{12} of SNe Ia with negligible host galaxy reddening on the decline rate Δm_{15}.

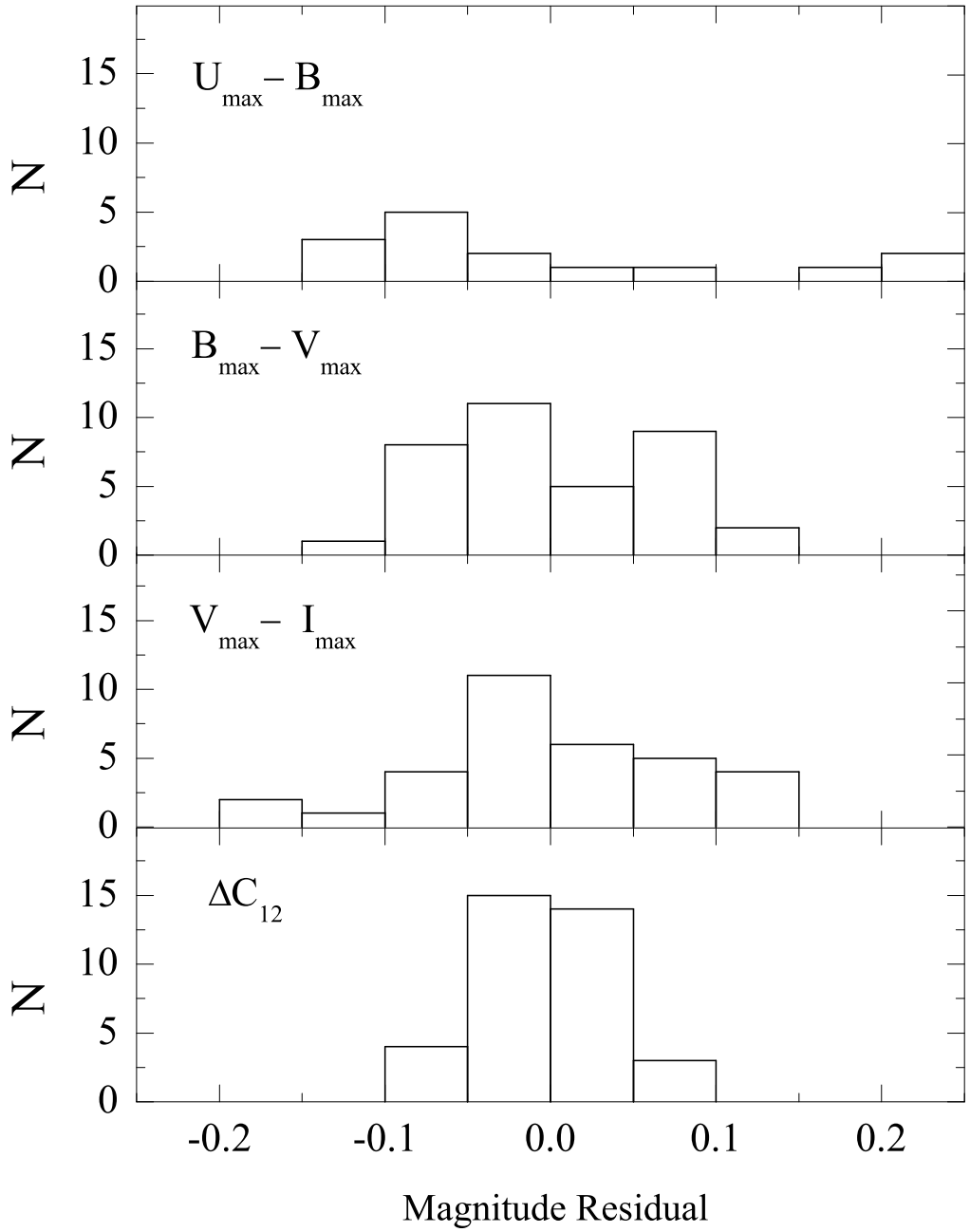

Fig. 2.— Histogram of the residual distribution for the fit to the color$-\Delta m_{15}$ relation as shown in Figure 1.

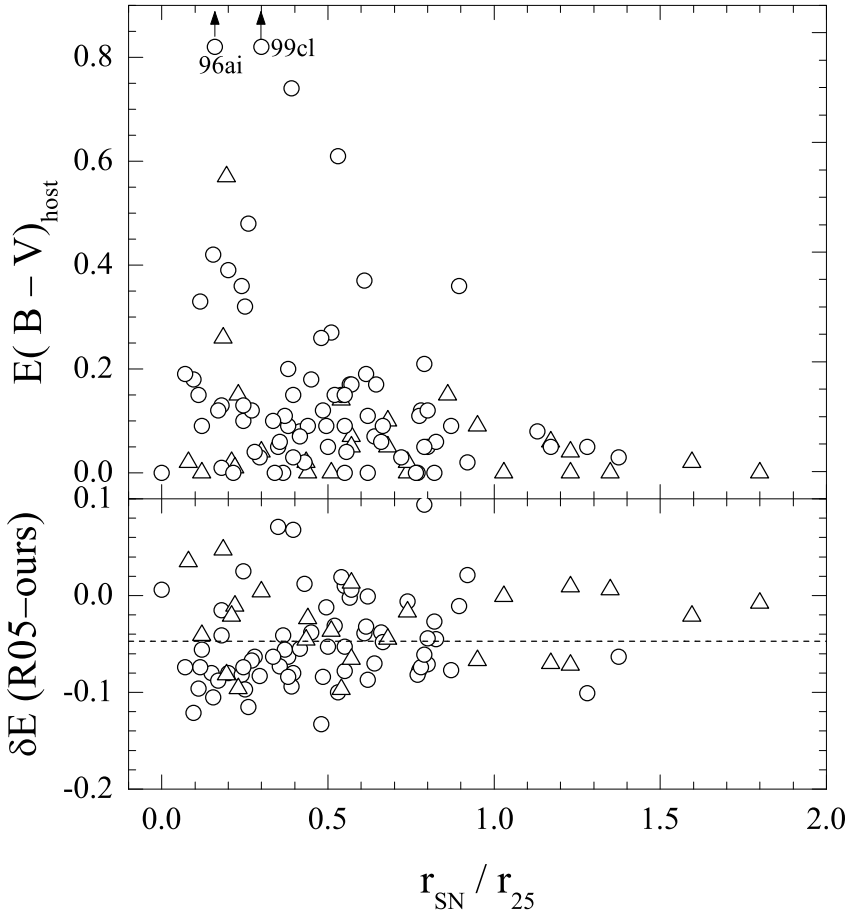

Fig. 3.— Top panel: Reddening distribution of SNe Ia in their respective host galaxies. The circles show the SNe Ia in spiral galaxies, and the triangles represent those in E/S0 galaxies. The two SNe 1996ai, 1999cl as marked by the arrows have the host galaxy reddening values of $E(B-V)_{host} = 1.69$ and 1.20, respectively. Bottom panel: Difference of the host galaxy reddening values as derived between R05 and this paper. The dashed line marks the mean value of the reddening difference.

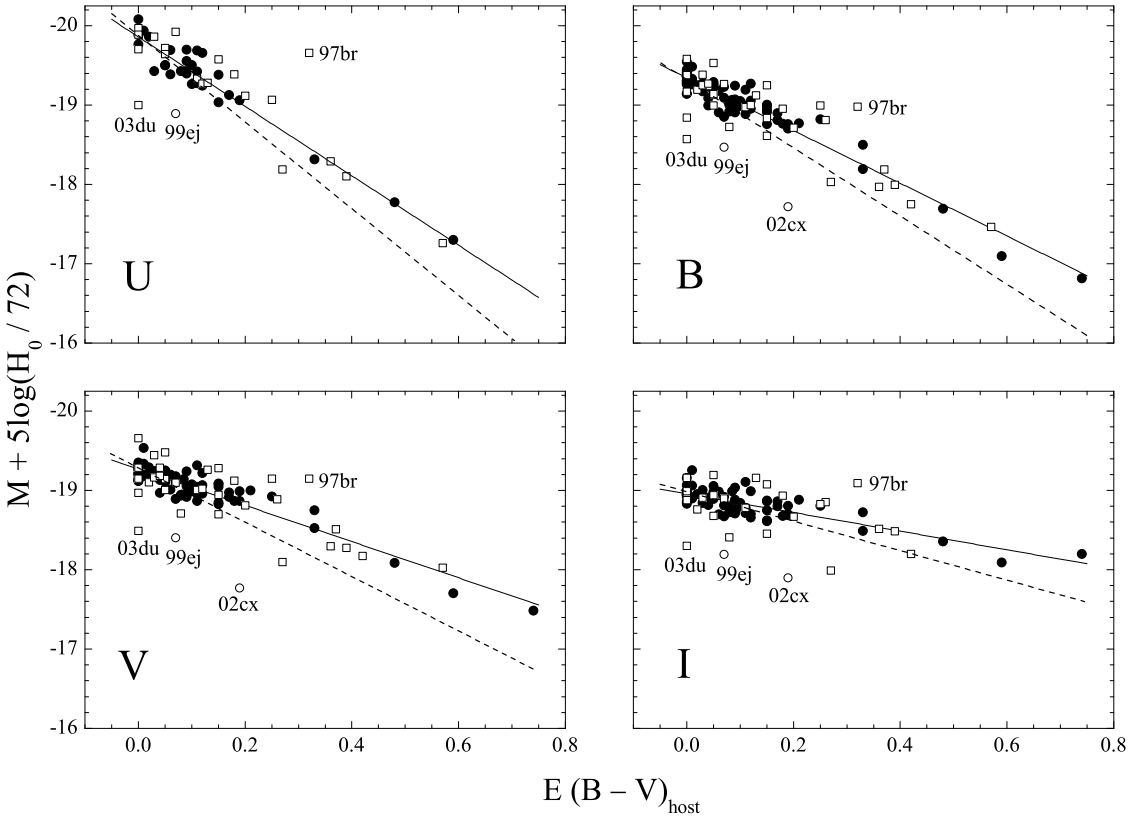

Fig. 4.— Dependence of the absolute magnitudes on the host galaxy reddening $E(B-V)_{host}$ for SNe Ia in $UBVI$ bands. The absolute magnitudes are corrected for the Galactic absorption and the intrinsic dependence on ΔC_{12}. The circles shown here are Hubble flow SN sample. The SNe Ia with $v \lesssim$3,000 km s^{-1}, represented by squares, are not included in the fits. The two most reddened SNe 1996ai, 1999cl are not shown for the space limit. The solid lines depict the best-fitting reddening vectors in distant galaxies, while the dashed lines show the canonical Galactic reddening vectors.

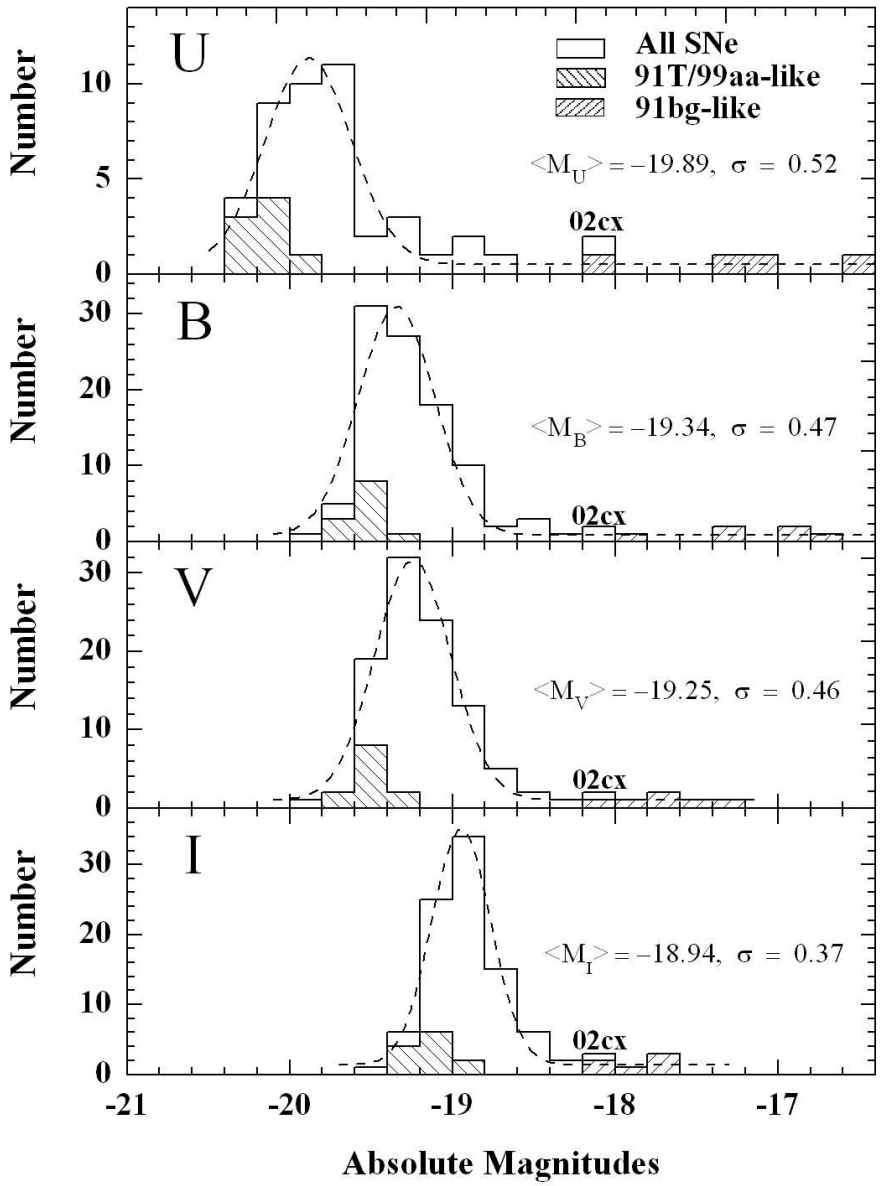

Fig. 5.— Distribution of the absolute magnitudes at maximum for 109 SNe Ia in $UBVI$ bands. Gaussian fit (the dashed lines) to the absolute magnitudes, the mean values and the standard deviations are also shown.

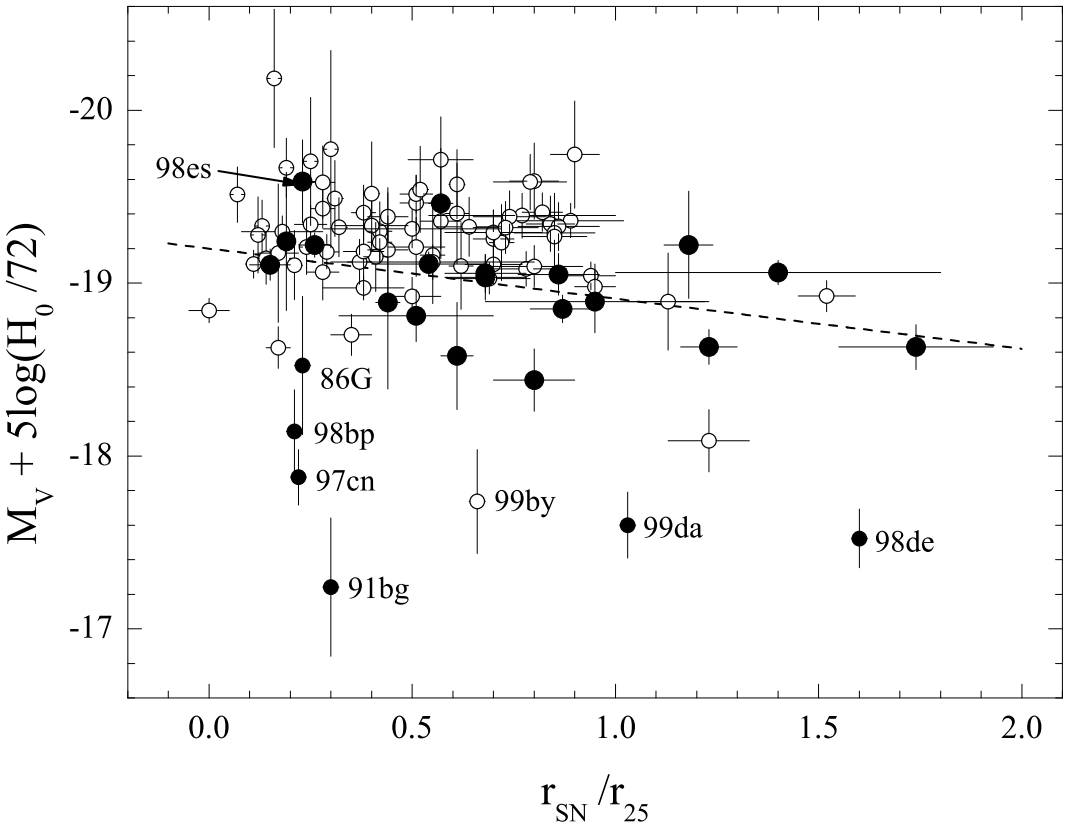

Fig. 6.— Absolute magnitudes M_V (fully corrected for the extinction) plotted against the relative radial distance r_{SN}/r_{25}. The open circles show the spirals and the filled circles represent the E/S0 galaxies. The larger filled circles are for the normal SNe Ia in E/S0.

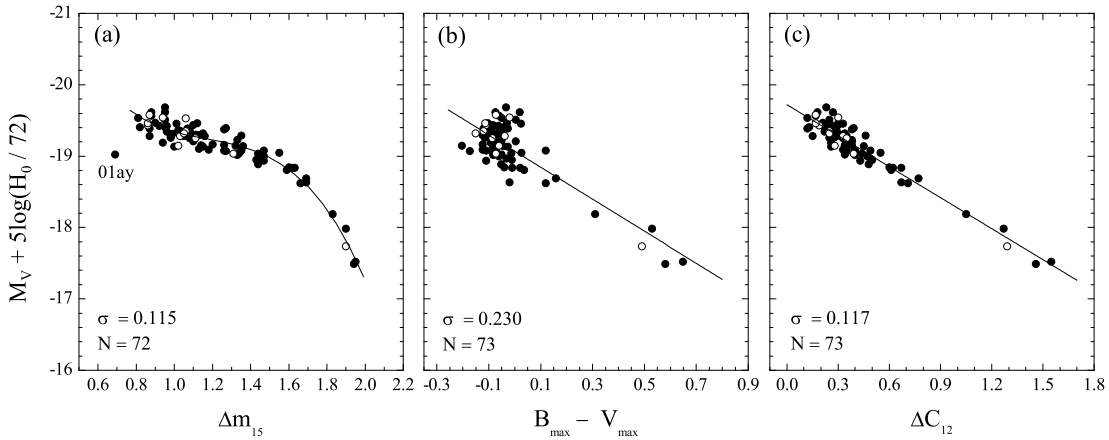

Fig. 7.— Absolute magnitudes M_V, fully corrected for extinction, versus the decline rate Δm_{15}, the peak color $B-V$, and the post-maximum color ΔC_{12}. Filled circles show the Hubble flow SN sample and the open circles represent the nearby calibrators.

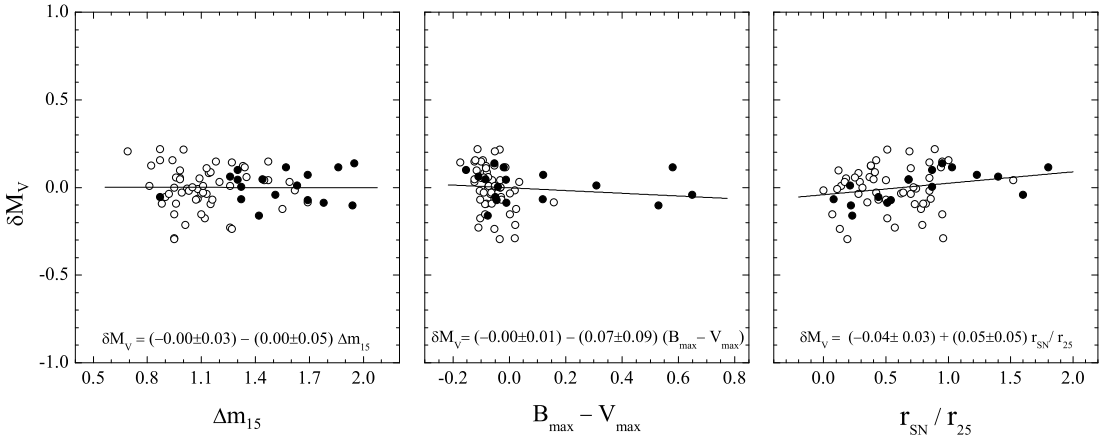

Fig. 8.— Residuals of the $M_V - \Delta C_{12}$ relation fits for M_V plotted against the decline rate Δm_{15}, the peak color $B_{max} - V_{max}$, and the location of the SNe Ia in their host galaxies. The open circles are for spiral galaxies, and the filled circles are for E/S0 galaxies.

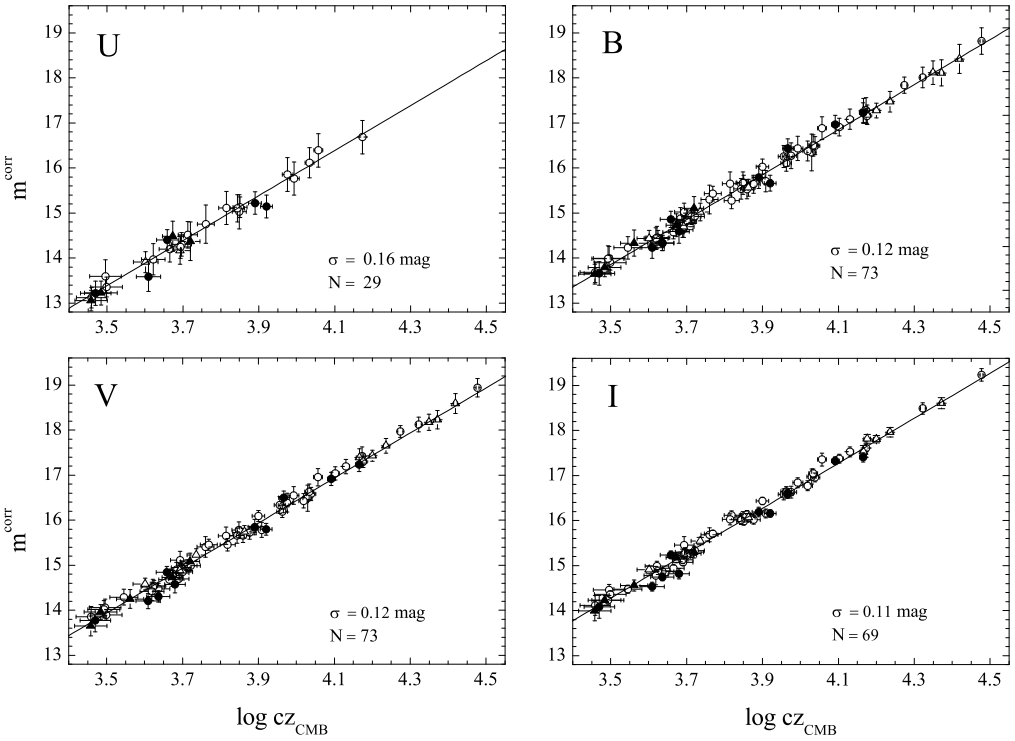

Fig. 9.— Hubble diagrams in U, B, V, and I for 73 SNe Ia with $0.01 \lesssim z \lesssim 0.1$, which were calibrated using ΔC_{12}. SNe Ia in spiral galaxies are shown with circles, while those in E/S0 galaxies are shown with triangles. Open symbols are for normal SNe Ia, and the filled symbols are for the spectroscopically peculiar events. The best-fit linear regressions are shown, with a dispersion of $\sim$0.16 mag in the U band, and $\lesssim$0.12 mag in the BVI bands.